Structure and thermodynamics of a ferrofluid bilayer

Carlos Alvarez,[1,2,3] Martial Mazars,[1,*] and Jean-Jacques Weis[1]
[1]*Laboratoire de Physique Théorique (UMR 8627), Université de Paris Sud XI, Bâtiment 210, 91405 Orsay Cedex, France*
[2]*Departamento de Fisica, Universidad de Los Andes, Carrera 1E# 18-10, Bogotá, Colombia*
[3]*Laboratoire de Physique Théorique et Modèles Statistiques (UMR 8626), Université de Paris Sud XI, Bâtiment 100, 91405 Orsay Cedex, France*
(Received 8 February 2008; published 9 May 2008)

We present extensive Monte Carlo simulations for the thermodynamic and structural properties of a planar bilayer of dipolar hard spheres for a wide range of densities, dipole moments, and layer separations. Expressions for the stress and pressure tensors of the bilayer system are derived. For all thermodynamic states considered, the interlayer energy is shown to be attractive and much smaller than the intralayer contribution to the energy. It vanishes at layer separations of the order of two hard sphere diameters. The normal pressure is negative and decays as a function of layer separation h as $-1/h^5$. Intralayer and interlayer pair distribution functions and angular correlation functions are presented. Despite the weak interlayer energy, strong positional and orientational correlations exist between particles in the two layers.

DOI: 10.1103/PhysRevE.77.051501 PACS number(s): 61.20.Gy, 68.15.+e, 75.10.−b, 75.40.Mg

I. INTRODUCTION

Dipolar interactions play a significant role in determining the structural, magnetic or rheological properties of a variety of quasi-two-dimensional (2D) systems (monolayers, multilayers, thin films) including suspensions of colloidal particles at an air-water interface, adsorbed amphiphilic molecules, lipid bilayers, ultrathin magnetic films, etc.. (see, e.g., Ref. [1] and references therein). In most of these systems the properties and phase behavior result, though, from an interplay of the dipolar interaction with competing interactions, such as, for instance, the hydrocarbon chain tails or water-mediated interactions in lipid bilayers [2,3], or exchange interaction and magnetocrystalline anisotropy in thin magnetic films [4]. Although simulations taking into account full atomic details have been performed in the past (generally computationally costly) for these kinds of systems (see, e.g., Ref. [5] and references therein), we believe that a study of a purely dipolar bilayer system is of interest in its own right, providing unbiased insight into the role of the dipolar interaction. The experimental system which perhaps comes closest to the pure dipolar system is the ferrofluid system. In effect, association into chains, rings, branched structures, or stripes has been demonstrated in recent experiments on strongly interacting (Fe_3O_4) ferrofluids [6–8], and comparison with simulation results presenting similar structures is more than suggestive that the dipolar hard sphere (DHS) system is a fair representation of these types of ferrofluid.

Extensive Monte Carlo (MC) simulation and theoretical results for the self-organization of quasi-2D DHSs are already available for the monolayer system both with and without an external field [9–18]. The purpose of the present paper is to extent these results to a symmetric planar bilayer; the main interest, evidently, being to probe the effect of the interlayer interaction on particle organization.

In Sec. II we define the bilayer model and give details of the numerical simulation methods we use. The next section gives expressions for the energy, stress tensor, and correlation functions of the bilayer system. Section IV contains the simulation results for the thermodynamic and structural properties. A summary is given in the last section. The three appendixes provide expressions for the Ewald sums of energy (Appendix A), pressure and forces (Appendix C), and a derivation of the microscopic stress tensor of the bilayer (Appendix B).

II. MODEL AND NUMERICAL METHODS

The systems consist of $N=2N_0$ particles with permanent point dipole moment μ interacting via hard sphere and dipolar potentials. Particles are evenly distributed among two layers L_1 and L_2 separated by a distance h, each layer being rectangular with sides L_x and L_y; $A=L_xL_y$ is the surface area of the layers. Periodic boundary conditions (PBCs), with spatial periodicities L_x and L_y, are applied in the directions x and y parallel to the layers, but no PBCs are taken in the third direction z. Particle positions are constrained to lie in the layers but dipole moments can orient in full 3D space. The interaction potential between the particles is pairwise additive and is represented as

$$\Phi(\boldsymbol{r}_{ij},\boldsymbol{\mu}_i,\boldsymbol{\mu}_j) = \begin{cases} \infty & \text{for } r_{ij}<\sigma, \\ \dfrac{1}{r_{ij}^3}[\boldsymbol{\mu}_i\cdot\boldsymbol{\mu}_j - 3(\boldsymbol{\mu}_i\cdot\hat{\boldsymbol{r}}_{ij})(\boldsymbol{\mu}_j\cdot\hat{\mathbf{r}}_{ij})] & \text{for } r_{ij}>\sigma, \end{cases} \tag{1}$$

where $\sigma=1$ is the hard sphere diameter taken as unit length, $\boldsymbol{\mu}_i$ the dipole moment of particle i, and $\hat{\boldsymbol{r}}_{ij}=\boldsymbol{r}_{ij}/r_{ij}$ the unit bond vector between particles i and j. In the following, we will use the notations

*Author to whom correspondence should be addressed. martial.mazars@th.u-psud.fr

$$\boldsymbol{r}_{ij} = \boldsymbol{s}_{ij} + z_{ij}\hat{\boldsymbol{e}}_z \quad \text{and} \quad \boldsymbol{\mu}_i = \mu\hat{\boldsymbol{\mu}}_i \tag{2}$$

where $\hat{\boldsymbol{e}}_z$ is the unit vector perpendicular to the layers and $\hat{\boldsymbol{\mu}}_i$ a unit vector in the direction of dipole moment i.

Only surface separations $h>1$ which avoid hard core interactions between the layers have been considered. A few simulation results for $h<1$ have been presented previously by one of us [1].

Monte Carlo simulations have been performed in the canonical (NVT) ensemble with system sizes comprising $N=1024-3200$ particles. The total number of MC cycles varied from 0.2×10^6 to 2×10^6, depending on density and dipole moment, each cycle consisting of displacement and rotation of the N particles. The amplitude of the trial moves was chosen to obtain acceptance ratios between 30% and 50% for each thermodynamic state. No exchange of particles between layers L_1 and L_2 is allowed.

Reduced quantities for surface area $A^*=A/\sigma^2$, surface density $\rho^*=\rho\sigma^2=N_0/A\sigma^2$, and dipole moment $\mu^*=(\mu^2/kT\sigma^3)^{1/2}$ will be used throughout the paper. For notational convenience the asterisks will be dropped.

III. THERMODYNAMICAL AND STRUCTURAL QUANTITIES

A. Energy

In our model the energy of the bilayer is entirely given by the dipolar contribution which we split into an intralayer contribution, U^{intra}, and an interlayer contribution, U^{inter}, as

$$U_{dd} = U^{\text{intra}} + U^{\text{inter}}. \tag{3}$$

These are computed using the Ewald method [1,19–21]; the relevant expressions for U^{intra} and U^{inter} are given in Appendix A.

For bulk systems with slab geometry where periodicity applies only in two spatial directions, say L_x and L_y, the Ewald sums are computationally costly, due to the appearance in the reciprocal space term of a double sum over the distance z_{ij} in the bounded direction of particles i and j [19,20]. As in the present case the distance z_{ij} between two particles will be constant; the corresponding sums can be reduced to order N [1] similarly to the cases of the Coulomb [22,23] or Yukawa [24] potentials.

One can note that the 3D bilayer system can be mapped onto a two-component monolayer system by considering the particles in the two layers as distinct species [25]. For most of the thermodynamical and structural quantities, both approaches are equivalent; for instance, in the two-component monolayer, U^{inter} is the total interaction between particles belonging to different species (different layers). As outlined in the next section and in Appendix B, for pressures and stresses such a mapping is slightly less straightforward.

B. Surface stress tensor and normal pressure

Characterizing the pressure in the bilayer system needs some care. In particular, since the particles are constrained to belong to layers L_1 and L_2, some degrees of freedom of the particles are frozen by the geometrical features of the system. These constraints have obviously an influence on the flux of momentum per unit area in the system and therefore affect the stress tensor. For the sake of definitness a full derivation of the stress tensor from the Lagrangian function of the bilayer system is given in Appendix B.

As for systems with slab geometry or interfaces [26], the stress tensor is decomposed into lateral and normal components. According to Eqs. (B13)–(B15), the lateral component to the pressure tensor is given by

$$\begin{aligned}\Pi_T = 2\rho kT &- \frac{1}{4A}\left\langle \sum_{i\in L_1}\sum_{j\in L_1, j\neq i} \boldsymbol{s}_{ij}\cdot\boldsymbol{\nabla}_i\Phi(\boldsymbol{s}_{ij},0)\right\rangle \\ &- \frac{1}{4A}\left\langle \sum_{i\in L_2}\sum_{j\in L_2, j\neq i} \boldsymbol{s}_{ij}\cdot\boldsymbol{\nabla}_i\Phi(\boldsymbol{s}_{ij},0)\right\rangle \\ &- \frac{1}{2A}\left\langle \sum_{i\in L_1}\sum_{j\in L_2} \boldsymbol{s}_{ij}\cdot\boldsymbol{\nabla}_i\Phi(\boldsymbol{s}_{ij},h)\right\rangle,\end{aligned} \tag{4}$$

where $\Phi(\boldsymbol{s}_{ij},h)$ is the pair potential.

From the point of view of mapping the bilayer system onto a two-component monolayer system, the lateral pressure Π_T in the bilayer, defined in Eq. (4) through Eqs. (B12)–(B15), corresponds to the pressure of the 2D, two-component monolayer system. In solid surface physics, Π_T is related to the surface stress $\tilde{\eta}$ by $\Pi_T=-\tilde{\eta}$ [cf. Eq. (B15)], and for fluids confined in slab geometry Π_T is related to the lateral pressure $P_T(z)$ by

$$\Pi_T = \int dz\, P_T(z).$$

Π_T can be composed into ideal, hard sphere (HS), and dipolar contributions

$$\Pi_T = 2\rho kT + 2\Pi_T^{(\text{HS})} + \Pi_{T,\text{inter}}^{(\text{HS})} + \Pi_T^{(dd)}, \tag{5}$$

where the dipolar part $\Pi_T^{(dd)}$ is obtained from Eq. (1) and the relation

$$\begin{aligned}s_{ij}^{\beta}\nabla_i^{\alpha}\Phi^{(dd)}(\boldsymbol{s}_{ij},h) &= 3\frac{s_{ij}^{\beta}s_{ij}^{\alpha}}{(s_{ij}^2+h^2)^{5/2}}\left[\boldsymbol{\mu}_i\cdot\boldsymbol{\mu}_j - 5\frac{(\boldsymbol{\mu}_i\cdot\boldsymbol{s}_{ij}+\mu_i^z h)(\boldsymbol{\mu}_j\cdot\boldsymbol{s}_{ij}+\mu_j^z h)}{s_{ij}^2+h^2}\right] \\ &\quad - 3\frac{s_{ij}^{\beta}}{(s_{ij}^2+h^2)^{5/2}}[(\boldsymbol{\mu}_i\cdot\boldsymbol{s}_{ij}+\mu_i^z h)\mu_j^{\alpha} \\ &\quad + (\boldsymbol{\mu}_j\cdot\boldsymbol{s}_{ij}+\mu_j^z h)\mu_i^{\alpha}]\end{aligned} \tag{6}$$

[see Eq. (B14) of Appendix B]. $\Pi_T^{(dd)}$ contains both intralayer contributions of layers L_1 and L_2 and the interlayer contribution; thus, for $h\to\infty$, $\Pi_T^{(dd)}$ is twice the dipolar contribution to the 2D pressure of a monolayer. The dipolar interlayer contribution to Π_T is given by the last contribution in the right-hand side (RHS) of Eq. (4); this contribution becomes very small as soon as $h\gtrsim 2$.

The hard sphere contributions $\Pi_T^{(\text{HS})}$ and $\Pi_{T,\text{inter}}^{(\text{HS})}$ are computed from the contact values of the intralayer, $g_{\text{intra}}^{000}(\sigma)$, and interlayer, g_{inter}^{000}, pair distribution functions, defined below, as

$$\Pi_T^{(\mathrm{HS})} = \frac{\pi}{2}\rho^2 kT g_{\mathrm{intra}}^{000}(\sigma),$$

$$\Pi_{T,\mathrm{inter}}^{(\mathrm{HS})} = \frac{\pi}{2}(2\rho)^2 kT g_{\mathrm{inter}}^{000}\left(\sigma\sqrt{1-\frac{h^2}{\sigma^2}}\right). \tag{7}$$

As in the present work, $h>1$ in all computations, we always have $\Pi_{T,\mathrm{inter}}^{(\mathrm{HS})}=0$. In the limit $h\to\infty$ and $\mu\to 0$, $\Pi_T^{(\mathrm{HS})}$ equals the excess contribution to the pressure of a monolayer of hard disks with surface density ρ. Moreover, for $h\geq 1$ and $\mu=0$, $\Pi_T^{(\mathrm{HS})}$ can be approximated quite accurately by available equations of state of hard disks (see, e.g., Ref. [27]).

The asymptotic behavior of Π_T given by Eq. (5) can be understood as follows. In the limit $h\to\infty$ and $\mu\neq 0$, Π_T, given by Eq. (5), is exactly twice the 2D pressure of a monolayer of DHSs with the same ρ and μ. In this limit, if the system is viewed as a two-component monolayer system, the two species remain distinct but there will be no interaction between particles belonging to different species. Thus, $\Pi_T/2$ is exactly the partial pressure of each component, and the bilayer is fully equivalent to a mixture of two kinds of particles confined in a monolayer with HS and dipolar interactions between like particles but no interactions between unlike particles.

In the opposite limit $h\to 0$ and $\mu\neq 0$, the two species become equal and the bilayer system reduces to a one-component monolayer system with a surface density 2ρ (provided that 2ρ is less than the density at close packing of hard disks). Obviously, in this limit, the contribution $\Pi_{T,\mathrm{inter}}^{(\mathrm{HS})}$ has also to be included in Eq. (5), and Π_T equals the 2D pressure of a monolayer of dipolar hard disks with a surface density 2ρ and the same μ. Also, as in this limit particles become indistinguishable, entropy contributions must be modified accordingly.

The average normal force by unit area (or normal pressure) is obtained from Eq. (B19) as

$$P_{zz} = -\frac{1}{A}\left\langle \frac{\partial}{\partial z}\sum_{i\in L_1}\sum_{j\in L_2}\Phi(\boldsymbol{s}_{ij},z)\big|_{z=h}\right\rangle$$
$$= -\frac{N}{A}\left\langle \frac{\partial \beta U^{\mathrm{inter}}/N}{\partial h}\right\rangle = P_{zz}^{(dd)} + P_{zz}^{(\mathrm{HS})}, \tag{8}$$

where $P_{zz}^{(dd)}$ and $P_{zz}^{(\mathrm{HS})}$ denote the contributions from dipolar and HS interactions, respectively. The dipolar parts $P_{zz}^{(dd)}$ and $\Pi_T^{(dd)}$ are computed using Ewald sums, as described in Appendix C. Since in the present work all computations are done with $h>1$ one has always $P_{zz}^{(\mathrm{HS})}=0$. The HS repulsion does, however, contribute to the normal component of the pressure tensor indirectly via the spatial positions of the particles in the layers. A similar remark applies to the interlayer correlation functions defined below. Equation (8) agrees with previous derivations for the normal pressure in slablike geometry [28–30] or interfaces [26]. The main difference between Eq. (8) and these relations is that there is no kinetic (ideal gas) contribution in Eq. (8), as a consequence of the constraints that apply to the bilayer systems [cf. Eq. (B7)]. Thus, P_{zz} has to be considered as an average force per unit area normal to the surface rather than a normal pressure.

The surface stress tensor is related to the surface free energy per unit area γ (or surface tension) by the Shuttleworth equation [31]

$$\eta_{\alpha\beta} = \gamma\delta_{\alpha\beta} + \frac{\partial\gamma}{\partial\epsilon_{\alpha\beta}}, \tag{9}$$

where $\epsilon_{\alpha\beta}$ is the 2D strain tensor. In fluid phases, the second contribution in the RHS of Eq. (9) is null and Eq. (9) reduces to $\eta_{\alpha\beta}=\gamma\delta_{\alpha\beta}$. This is the case in most computations done in the present work, except those at high densities. Since in our computations the surface and the shape of the layers are kept constant, we do not have access to γ.

C. Correlation functions

The structure of the bilayer system has been characterized, analogously to the monolayer case [9,14] by a one-particle orientational distribution function of the dipoles and several pair correlation functions.

The orientational distribution function $f(\hat{\boldsymbol{\mu}})$, measuring the orientation of the particle dipole moments with respect to the layer normal, is defined from the one-body density as

$$\rho^{(1)}(\boldsymbol{r},\hat{\boldsymbol{\mu}}) = \left\langle \sum_i \delta(\boldsymbol{r}_i-\boldsymbol{r})\delta(\hat{\boldsymbol{\mu}}_i-\hat{\boldsymbol{\mu}})\right\rangle = \frac{\rho}{4\pi}f(\hat{\boldsymbol{\mu}}). \tag{10}$$

Pair correlation functions are derived from the general definition of the two-body density

$$\rho^{(2)}(\boldsymbol{r},\boldsymbol{r}',\hat{\boldsymbol{\mu}},\hat{\boldsymbol{\mu}}')$$
$$= \left\langle \sum_{i\neq j}^{N}\delta(\boldsymbol{r}_i-\boldsymbol{r})\delta(\boldsymbol{r}_j-\boldsymbol{r}')\delta(\hat{\boldsymbol{\mu}}_i-\hat{\boldsymbol{\mu}})\delta(\hat{\boldsymbol{\mu}}_j-\hat{\boldsymbol{\mu}}')\right\rangle, \tag{11}$$

where $\hat{\boldsymbol{\mu}}$ and $\hat{\boldsymbol{\mu}}'$ are unit vectors along the dipole moments. Specifying to intralayer $\rho_{\mathrm{intra}}^{(2)}$ and interlayer $\rho_{\mathrm{inter}}^{(2)}$ two-body surface densities, one has

$$\rho_{\mathrm{intra}}^{(2)}(s,\hat{\boldsymbol{\mu}},\hat{\boldsymbol{\mu}}')$$
$$= \frac{1}{4\pi s}\left\langle \sum_{i\in L_1}\sum_{j\in L_1, j\neq i}\delta(s-|\boldsymbol{s}_{ij}|)\delta(\hat{\boldsymbol{\mu}}_i-\hat{\boldsymbol{\mu}})\delta(\hat{\boldsymbol{\mu}}_j-\hat{\boldsymbol{\mu}}')\right.$$
$$\left. + \sum_{i\in L_2}\sum_{j\in L_2, j\neq i}\delta(s-|\boldsymbol{s}_{ij}|)\delta(\hat{\boldsymbol{\mu}}_i-\hat{\boldsymbol{\mu}})\delta(\hat{\boldsymbol{\mu}}_j-\hat{\boldsymbol{\mu}}')\right\rangle,$$

$$\rho_{\mathrm{inter}}^{(2)}(s,\hat{\boldsymbol{\mu}},\hat{\boldsymbol{\mu}}')$$
$$= \frac{1}{2\pi s}\left\langle \sum_{i\in L_1}\sum_{j\in L_2}\delta(s-|\boldsymbol{s}_{ij}|)\delta(\hat{\boldsymbol{\mu}}_i-\hat{\boldsymbol{\mu}})\delta(\hat{\boldsymbol{\mu}}_j-\hat{\boldsymbol{\mu}}')\right\rangle. \tag{12}$$

The intralayer $g_{\mathrm{intra}}(12)$ and interlayer $g_{\mathrm{inter}}(12)$ distribution functions are related to the two-body densities through

$$g_{\mathrm{intra}}(12) = 1 + h_{\mathrm{intra}}(12) = \left(\frac{4\pi}{\rho}\right)^2\rho_{\mathrm{intra}}^{(2)}(s,\hat{\boldsymbol{\mu}}_1,\hat{\boldsymbol{\mu}}_2),$$

$$g_{\mathrm{inter}}(12) = 1 + h_{\mathrm{inter}}(12) = \left(\frac{4\pi}{\rho}\right)^2\rho_{\mathrm{inter}}^{(2)}(s,\hat{\boldsymbol{\mu}}_1,\hat{\boldsymbol{\mu}}_2). \tag{13}$$

In particular, the intralayer $g_{\mathrm{intra}}^{000}(s)$ and interlayer $g_{\mathrm{inter}}^{000}(s)$ center-to-center pair distribution functions are given by

TABLE I. Definitions of the projections of intralayer and interlayer correlation functions computed in the present work.

(l_1,l_2,l)	$\tilde{\Phi}^{l_1l_2l}$	Intralayer and interlayer functions
(0,0,0)	1	$g^{000}_{\text{intra,inter}}(s)=\langle g_{\text{intra,inter}}(12)\rangle_{\hat{\boldsymbol{\mu}}_1\hat{\boldsymbol{\mu}}_2}$
(1,1,0)	$\hat{\boldsymbol{\mu}}_1\cdot\hat{\boldsymbol{\mu}}_2$	$h^{110}_{\text{intra,inter}}(s)=3\langle g_{\text{intra,inter}}(12)\tilde{\Phi}^{110}(12)\rangle_{\hat{\boldsymbol{\mu}}_1\hat{\boldsymbol{\mu}}_2}$
(1,1,2)	$3(\hat{\boldsymbol{\mu}}_1\cdot\hat{\boldsymbol{r}})(\hat{\boldsymbol{\mu}}_2\cdot\hat{\boldsymbol{r}})-\hat{\boldsymbol{\mu}}_1\cdot\hat{\boldsymbol{\mu}}_2$	$h^{112}_{\text{intra,inter}}(s)=\frac{3}{2}\langle g_{\text{intra,inter}}(12)\tilde{\Phi}^{112}(12)\rangle_{\hat{\boldsymbol{\mu}}_1\hat{\boldsymbol{\mu}}_2}$
(2,2,0)	$\frac{1}{2}[3(\hat{\boldsymbol{\mu}}_1\cdot\hat{\boldsymbol{\mu}}_2)^2-1]$	$h^{220}_{\text{intra,inter}}(s)=\frac{5}{2}\langle g_{\text{intra,inter}}(12)\tilde{\Phi}^{220}(12)\rangle_{\hat{\boldsymbol{\mu}}_1\hat{\boldsymbol{\mu}}_2}$

$$g^{000}_{\text{intra}}(s)=\frac{1}{4\pi s\rho N_0}\left\langle \sum_{i\in L_1}\sum_{j\in L_1,j\neq i}\delta(s-|\boldsymbol{s}_{ij}|)+\sum_{i\in L_2}\sum_{j\in L_2,j\neq i}\delta(s-|\boldsymbol{s}_{ij}|)\right\rangle=\langle g_{\text{intra}}(12)\rangle_{\hat{\boldsymbol{\mu}}_1\hat{\boldsymbol{\mu}}_2},$$

$$g^{000}_{\text{inter}}(s)=\frac{1}{2\pi s\rho N_0}\left\langle \sum_{i\in L_1}\sum_{j\in L_2}\delta(s-|\boldsymbol{s}_{ij}|)\right\rangle=\langle g_{\text{inter}}(12)\rangle_{\hat{\boldsymbol{\mu}}_1\hat{\boldsymbol{\mu}}_2}, \tag{14}$$

where $\boldsymbol{s}_i$ is the in-plane position of particle i according to the notations defined in Eq. (2) and $\langle\cdot\rangle_{\hat{\boldsymbol{\mu}}_1\hat{\boldsymbol{\mu}}_2}$ denotes averaging over orientations of the dipole moments. The angular-dependent pair correlation functions $h(12)$ have been expanded, as usual, on a basis set of rotational invariants $\tilde{\Phi}^{l_1l_2l}$ [32,33]

$$h(12)=\sum_{l_1,l_2,l}h(l_1,l_2,l;r)\tilde{\Phi}^{l_1l_2l}(\hat{\boldsymbol{\mu}}_1,\hat{\boldsymbol{\mu}}_2,\hat{\boldsymbol{r}}), \tag{15}$$

where the $\tilde{\Phi}^{l_1l_2l}$ are related to the standard rotational invariants $\Phi^{l_1l_2l}$ in an expansion on spherical harmonics by (see, e.g., [34])

$$\tilde{\Phi}^{l_1l_2l}=\frac{1}{l!}\begin{pmatrix}l_1 & l_2 & l\\ 0 & 0 & 0\end{pmatrix}\Phi^{l_1l_2l}. \tag{16}$$

The most significant projections of the intralayer $h_{\text{intra}}(12)$ and interlayer $h_{\text{inter}}(12)$ correlation functions calculated in this work are those onto $\tilde{\Phi}^{110}$, $\tilde{\Phi}^{112}$, and $\tilde{\Phi}^{220}$. The corresponding expressions are summarized in Table I.

D. Order parameter

Possible orientational (nematic) order in a layer can be established from the nonvanishing of the second-rank order parameter P_2 calculated as the average value of the largest eigenvalue of the matrix [37]

$$Q_{\alpha\beta}=\frac{1}{N_0}\sum_{i}^{N_0}\frac{1}{2}(3\hat{\mu}^i_\alpha\hat{\mu}^i_\beta-\delta_{\alpha\beta}), \tag{17}$$

where $\hat{\mu}^i_\alpha$ is the α component of the unit vector $\hat{\boldsymbol{\mu}}_i$. One can note that the projection h^{220} obeys the asymptotic relationship

$$h^{220}(s)\sim 5P_2^2,\quad s\to\infty. \tag{18}$$

As will be shown below no global nematic order occurs in the systems for $\rho<0.7$.

IV. RESULTS

A. One-body orientational distribution function

One-body distribution functions $f(\hat{\boldsymbol{\mu}})=f(\cos(\theta))$, with polar angle θ defined by $\cos\theta=\hat{\boldsymbol{\mu}}\cdot\hat{\boldsymbol{e}}_z$, obtained from MC simulation at various thermodynamic states are shown in Fig. 1(a). It is seen that for all states an excellent fit to the MC data is obtained with the one-parameter function

$$f(\cos\theta;a)=f_0\exp(-a\cos^2\theta) \tag{19}$$

with normalization constant

$$f_0=\sqrt{\frac{a}{\pi}}\frac{1}{\text{erf}(\sqrt{a})}. \tag{20}$$

Values of a obtained by fitting the MC histograms $P(\cos\theta)$, normalized to 1, are given in Tables II–IV. The results for the orientational distribution functions of the bilayer system are quite similar to those obtained earlier for monolayers [12]. As μ increases the dipole moments tilt more and more into the layer plane ($\cos\theta\sim 0$). The interaction between the two layers induces, though, a slight effect, in comparison to the monolayer system, as seen in Fig. 1(b) showing the variation of the orientational distributions with interlayer separation h for $\rho=0.7$ and $\mu=2.00$. As the separation between the layers decreases, the coupling between layers increases, which entails a slight tendency of the dipoles to orient perpendicularly to the plane. As a consequence the distributions are slightly broadened (the value of a decreases).

B. Energy

The variation of the intralayer $\beta U^{\text{intra}}/N$ and interlayer $\beta U^{\text{inter}}/N$ energies as a function of layer separation are summarized in Table II for the density $\rho=0.7$ and the two dipole moments $\mu=1$ and 2. The intralayer energy is seen to be by far the dominant contribution and is nearly independent of h, especially at the largest dipole moments where in-plane orientation of the dipole moments is prevalent. The interlayer energy is much smaller and decreases rapidly with layer separation vanishing at $h\approx 2$. The total energy remains practically constant when h varies from 1.05 to 2.0.

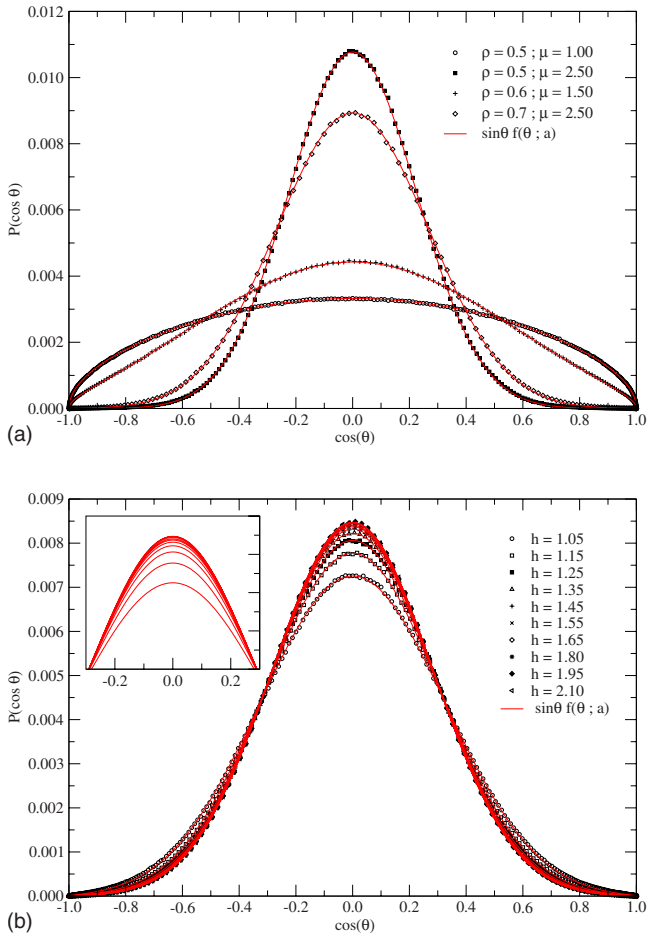

FIG. 1. (Color online) Orientational distribution functions of dipolar moments in a bilayer of dipolar hard spheres. Symbols denote MC data and solid lines are fits using Eq. (19). (a) Results at selected values of ρ and μ at $h=1.05$. (b) Variation with layer separation h for $\rho=0.7$ and $\mu=2.00$.

Attard and Mitchell have applied a second-order perturbation theory on a bilayer of orientable dipoles [35,36] and found that the interaction free energy between the surfaces decays as the fourth power of h at large separation. An analysis of our MC data, for $h \gtrsim 1.6$, agrees with the behavior obtained in the computations done by Attard and Mitchell; more precisely, the variation of the interlayer energy with h, for $\rho=0.7$ and $\mu=1$ and 2, can be quite well represented by

$$\frac{\beta U^{\text{inter}}}{N} = -\frac{e_0}{h^4} - \frac{e_1}{h^{10}}, \tag{21}$$

where e_0 and e_1 are obtained by a fit to the simulation results [see Fig. 2(a)].

Table III summarizes energy values obtained at fixed layer separation $h=1.05$ for various dipole moments in the density range $\rho=0.3-0.7$. For all densities considered the intralayer energy decreases with decreasing μ and saturates near $\mu \approx 2.5$. The variation with density diminishes when the dipole moment is increased. The interlayer energy is much smaller than the intralayer contribution presenting, at all densities, a shallow minimum in the range $\mu \approx 1.75-2.0$ where appreciable chaining of the particles sets in.

C. Pressure and surface stress

Similar to the interlayer energy, the normal pressure at constant μ and ρ is quite well represented, as a function of h, by

$$P_{zz} = -\frac{f_0}{h^5} - \frac{f_1}{h^{11}}. \tag{22}$$

However, as for a thermodynamical variable X generally

$$\left\langle \frac{\partial X}{\partial h} \right\rangle \neq \frac{\partial \langle X \rangle}{\partial h},$$

the fitting parameters f_0 and f_1 for the pressure do not relate directly to those for the energy. Nevertheless, the functional form of Eq. (22) obtained as the derivative of Eq. (21) provides quite good agreement between simulation results and Eq. (22) [see Fig. 2(b)].

As seen in Table II, the surface stress, for $\rho=0.7$, is fairly independent of h for $\mu=1$ and 2. For $\mu=1$, all the thermodynamic quantities $\Pi_T^{(dd)}$ and $\Pi_T^{(\text{HS})}$ that contribute to $\tilde{\eta}$ through Eqs. (B15) and (5) are nearly constant. For $\mu=2$, $\tilde{\eta}$ appears also to be insensitive to h, but a small counterbalance between $\Pi_T^{(dd)}$ and $\Pi_T^{(\text{HS})}$ is observed as h increases from 1.01 to 1.15. As apparent from the one-body orientational distribution functions, for h between 1.01 and 1.15 and $\mu=2$, the dipoles are on average less parallel to the layers than would be the case for larger h values. Thus, the attraction between particles in the same layer is slightly decreased in comparison to a monolayer; this increases $\Pi_T^{(dd)}$ and reduces $\Pi_T^{(\text{HS})}$, since fewer contacts between particles are observed in $g_{\text{intra}}^{000}(\sigma)$. One should note, though, that this effect is quite small (see Table II).

The values of $\tilde{\eta}$, for $\mu=1$, $\rho=0.7$, and $h>2.00$, given in Table II, agree with the results obtained for the 2D pressure of the monolayer (see Tables I and II in Ref. [14]). As outlined in Sec. III B, the value of Π_T obtained from $\tilde{\eta}$ is twice the value of the pressure found in Ref. [14]).

As shown previously, the 2D pressure of a monolayer of DHSs may be related to the internal energy of the monolayer [see Eq. (21) in Ref. [14]). For the bilayer, we obtain almost exactly the same result, except for a factor of 2 discussed before in Sec. III B. In Fig. 3(a), we have represented $-\Pi_T^{(dd)}$ as a function of $-U^{intra}/A$; it appears that the dipolar contribution to the lateral pressure of the bilayer is very well represented by

$$\Pi_T^{(dd)} = 3\rho kT \frac{\beta U^{\text{intra}}}{N} = 3\frac{U^{\text{intra}}}{A}. \tag{23}$$

Thus, for $\rho \leq 0.7$ and $\mu \leq 2.5$, the equation of state is given by an equation similar to Eq. (21) of Ref. [14] as

TABLE II. Average energies and pressures for the bilayer system for $\rho=0.7$ and several values of h. The numbers in brackets give the accuracy on the last digit of the averages. a is the width of the one-body orientational distribution obtained by fitting the MC histograms. $\beta U_{dd}/N$, $\beta U^{\text{intra}}/N$, and $\beta U^{\text{inter}}/N$ denote, respectively, the averages of total, intralayer, and interlayer dipolar energies. $P_{zz}^{(dd)}$ is the average normal force per unit area as defined by Eq. (7). $\Pi_T^{(dd)}$ is the average of the dipolar contribution to the lateral pressure computed with Eq. (4) and $\Pi_T^{(\text{HS})}$ is the hard sphere contribution computed from the contact value of the pair distribution function Eq. (6). $\tilde{\eta}=-2\rho kT-2\Pi_T^{(\text{HS})}-\Pi_T^{(dd)}$ is the surface stress as defined in Eq. (B15).

μ	h	a	$\beta U_{dd}/N$	$\beta U^{intra}/N$	$\beta U^{inter}/N$	$P_{zz}^{(dd)}$	$\Pi_T^{(dd)}$	$\Pi_T^{(HS)}$	$\tilde{\eta}$
1.00	1.05	0.36	−0.70(2)	−0.55(2)	−0.16(1)	−0.44(4)	−1.24(5)	3.2(2)	−6.6(2)
	1.15	0.43	−0.67(2)	−0.57(2)	−0.10(1)	−0.26(3)	−1.25(4)	3.1(1)	−6.4(1)
	1.25	0.48	−0.65(2)	−0.58(2)	−0.07(1)	−0.17(2)	−1.26(4)	3.1(1)	−6.3(1)
	1.35	0.52	−0.64(2)	−0.59(2)	−0.05(1)	−0.11(1)	−1.27(4)	3.1(1)	−6.3(1)
	1.45	0.52	−0.63(2)	−0.59(2)	−0.04(1)	−0.07(1)	−1.28(4)	3.2(1)	−6.5(1)
	1.55	0.53	−0.62(2)	−0.60(2)	−0.03(1)	−0.05(1)	−1.27(3)	3.1(1)	−6.3(1)
	1.65	0.57	−0.62(2)	−0.60(2)	−0.021(5)	−0.03(1)	−1.27(4)	3.1(1)	−6.3(1)
	1.80	0.55	−0.62(2)	−0.60(2)	−0.015(4)	−0.02(1)	−1.29(4)	3.1(1)	−6.3(1)
	1.95	0.57	−0.62(2)	−0.61(2)	−0.011(3)	−0.015(5)	−1.29(4)	3.1(1)	−6.3(1)
	2.10	0.57	−0.62(2)	−0.61(2)	−0.008(3)	−0.010(4)	−1.28(4)	3.2(1)	−6.5(1)
	2.40	0.57	−0.61(2)	−0.61(2)	−0.005(2)	−0.005(3)	−1.27(4)	3.1(1)	−6.3(1)
	3.00	0.58	−0.61(2)	−0.61(2)	−0.003(2)	−0.002(1)	−1.26(4)	3.2(1)	−6.5(1)
2.00	1.01	3.8	−6.3(1)	−5.7(1)	−0.56(4)	−1.8(1)	−12.2(1)	6.5(3)	−2.2(4)
	1.05	4.2	−6.3(1)	−5.8(1)	−0.42(3)	−1.3(1)	−12.5(1)	6.8(3)	−2.5(4)
	1.10	4.6	−6.3(1)	−5.9(1)	−0.32(3)	−0.9(1)	−12.7(1)	6.8(3)	−2.3(4)
	1.15	4.8	−6.3(1)	−6.1(1)	−0.24(2)	−0.6(1)	−12.8(1)	7.0(3)	−2.6(4)
	1.25	5.2	−6.3(1)	−6.1(1)	−0.16(2)	−0.32(3)	−13.0(1)	7.0(3)	−2.4(4)
	1.35	5.4	−6.3(1)	−6.2(1)	−0.11(1)	−0.20(2)	−13.1(1)	7.1(3)	−2.5(4)
	1.45	5.5	−6.3(1)	−6.2(1)	−0.08(1)	−0.13(2)	−13.1(1)	7.1(3)	−2.5(4)
	1.55	5.6	−6.3(1)	−6.21(5)	−0.06(1)	−0.09(2)	−13.2(1)	7.1(3)	−2.4(4)
	1.65	5.6	−6.3(1)	−6.23(5)	−0.05(1)	−0.06(1)	−13.2(1)	7.1(3)	−2.4(4)
	1.80	5.7	−6.3(1)	−6.25(5)	−0.03(1)	−0.03(1)	−13.1(1)	7.1(3)	−2.5(4)
	1.95	5.7	−6.3(1)	−6.28(5)	−0.02(1)	−0.03(1)	−13.3(1)	7.1(3)	−2.3(4)
	2.10	5.7	−6.3(1)	−6.28(5)	−0.019(5)	−0.019(5)	−13.2(1)	7.1(3)	−2.4(4)

$$\frac{\Pi_T}{2\rho kT}=1+\frac{\Pi_T^{(\text{HS})}}{\rho kT}+\frac{3}{2}\frac{\beta U^{\text{intra}}}{N}=-\frac{\tilde{\eta}}{2\rho kT}. \tag{24}$$

The variation of $\tilde{\eta}$ with dipole moment is shown in Fig. 3(b) for $h=1.05$ and various densities. $\tilde{\eta}$ can be approximated empirically by relations such as

$$\tilde{\eta}(\rho,\mu)=-2\rho kT-2\Pi_T^{(\text{HS})}(\rho,0)+g(a_1;\rho,\mu), \tag{25}$$

where $g(a_1;\rho,\mu)$ is a function of the fitting parameter a_1 and $\Pi_T^{(\text{HS})}(\rho,0)$ obtained from the equation of state of hard disks (see, for instance, Ref. [27]). Several functional forms for g, such as, for instance, $g_1(a_1;\rho,\mu)=a_1\rho^2\mu^4/(1+\mu^2)$, with $a_1\sim 2.7$, or $g_2(a_2;\rho,\mu)=a_2\rho^2\mu^{5/2}$, with $a_2\sim 1.6$, were found to reproduce quite accurately the numerical results given in Table IV.

D. Structural properties

Structural properties of the bilayer can be conveniently characterized by the coefficients g^{000}, h^{110}, h^{112}, and h^{220} of the expansion of the intra- and interlayer pair correlation functions $h_{\text{intra}}(1,2)$ and $h_{\text{inter}}(1,2)$ on a set of rotational invariants as described in Sec. III C. Selected results for both intra- and interlayer correlation functions for $h=1.05$ at densities $\rho=0.3$ and 0.7 are shown in Figs. 4–6. The intralayer correlation functions for $\mu=1$, reported in Fig. 4, agree very well with the correlation functions of the monolayer for the same ρ and for $\mu=1$ (see Fig. 4 of Ref. [14]).

The intralayer correlation functions present a succession of well-defined peaks reflecting the formation of chains as also apparent from snapshots of configurations [Figs. 7(a) and 7(b)]. The peaks sharpen with increasing dipole moment, indicating stronger bonding of the particles in the chains. The intralayer correlations appear to be quite insensitive to the layer separation and coincide within statistical error in the range $h=1.05-2.0$.

The interlayer correlation function gives information on the organization of particles in one layer relative to those in the other layer. Although the energy coupling between the layers is quite small, one observes a strong correlation of the positional and orientational order of the particles in the two layers (at least for $h<2$). Inspection of the interlayer distribution function g_{inter}^{000} reveals, for dipole moments $\mu\gtrsim 2$, a high probability of the particles to be on top of each other

TABLE III. Average energies for the bilayer system for several values of ρ and μ for $h=1.05$. Notations are the same as in Table II.

μ	ρ	$\beta U_{dd}/N$	$\beta U^{\text{intra}}/N$	$\beta U^{\text{inter}}/N$	a	μ	ρ	$\beta U_{dd}/N$	$\beta U^{\text{intra}}/N$	$\beta U^{\text{inter}}/N$	a
1.00	0.3	−0.29(1)	−0.19(1)	−0.10(1)	0.07	2.00	0.3	−4.9(1)	−4.3(1)	−0.52(3)	3.1
	0.4	−0.39(2)	−0.26(2)	−0.12(1)	0.12		0.4	−5.2(1)	−4.7(1)	−0.50(3)	3.4
	0.5	−0.49(2)	−0.35(2)	−0.14(1)	0.18		0.5	−5.6(1)	−5.1(1)	−0.48(4)	3.6
	0.6	−0.59(2)	−0.44(2)	−0.15(1)	0.25		0.6	−5.8(1)	−5.4(1)	−0.46(3)	3.8
	0.7	−0.70(2)	−0.54(2)	−0.16(1)	0.35		0.7	−6.3(1)	−5.8(1)	−0.42(4)	4.2
1.25	0.3	−0.68(2)	−0.46(2)	−0.22(2)	0.19	2.25	0.3	−8.1(1)	−7.8(1)	−0.34(3)	6.3
	0.4	−0.87(3)	−0.62(3)	−0.25(2)	0.31		0.4	−8.3(1)	−7.9(1)	−0.35(3)	6.3
	0.5	−1.06(3)	−0.80(3)	−0.27(2)	0.44		0.5	−8.4(1)	−8.0(1)	−0.38(3)	6.2
	0.6	−1.26(3)	−0.99(3)	−0.27(2)	0.60		0.6	−8.6(1)	−8.2(1)	−0.39(4)	6.2
	0.7	−1.46(3)	−1.19(3)	−0.27(2)	0.78		0.7	−8.9(1)	−8.6(1)	−0.39(3)	6.4
1.50	0.3	−1.38(4)	−1.01(4)	−0.37(2)	0.51	2.50	0.3	−11.7(1)	−11.5(1)	−0.20(2)	9.9
	0.4	−1.70(4)	−1.29(4)	−0.41(2)	0.71		0.4	−11.7(1)	−11.5(1)	−0.25(2)	9.6
	0.5	−2.00(4)	−1.59(4)	−0.41(2)	0.95		0.5	−11.8(1)	−11.5(1)	−0.28(3)	9.4
	0.6	−2.29(5)	−1.89(5)	−0.39(3)	1.2		0.6	−11.9(1)	−11.6(1)	−0.32(1)	9.2
	0.7	−2.60(5)	−2.22(5)	−0.37(3)	1.5		0.7	−12.2(1)	−11.9(1)	−0.34(2)	9.2
1.75	0.3	−2.65(5)	−2.13(5)	−0.52(3)	1.3						
	0.4	−3.1(1)	−2.5(1)	−0.52(3)	1.6						
	0.5	−3.4(1)	−2.9(1)	−0.50(4)	1.9						
	0.6	−3.8(1)	−3.3(1)	−0.46(3)	2.3						
	0.7	−4.2(1)	−3.8(1)	−0.42(3)	2.6						

with opposite directions of the dipole moments (h^{110}_{inter} negative at $s=0$). In addition, at dipole moments $\mu \gtrsim 2.25$, peaks appear in g^{000}_{inter} at $s=(0.5+n)\sigma$ $(n=0,1,2,\ldots)$ at which h^{110}_{inter} is positive, giving evidence for configurations in which two chains in different layers are nearly on top of each other (with possibly some lateral displacement) such that the chain axes of the two chains are displaced by half a HS diameter. In this case the dipole moments point in the same direction.

TABLE IV. Average pressures for the bilayer system for several values of ρ and μ for $h=1.05$. Notations are the same as in Table II.

μ	ρ	$P^{(dd)}_{zz}$	$\Pi^{(dd)}_T$	$\Pi^{(\text{HS})}_T$	$\tilde{\eta}$	μ	ρ	$P^{(dd)}_{zz}$	$\Pi^{(dd)}_T$	$\Pi^{(\text{HS})}_T$	$\tilde{\eta}$
1.00	0.3	−0.12(1)	−0.20(1)	0.26(1)	−0.92(2)	2.00	0.3	−0.62(4)	−4.0(1)	1.8(1)	−0.2(2)
	0.4	−0.20(2)	−0.36(2)	0.55(3)	−1.54(5)		0.4	−0.80(5)	−5.9(1)	2.7(1)	−0.3(2)
	0.5	−0.28(3)	−0.59(3)	1.02(5)	−2.4(1)		0.5	−1.0(1)	−7.9(1)	3.7(2)	−0.5(2)
	0.6	−0.36(3)	−0.87(3)	1.8(1)	−3.9(1)		0.6	−1.2(1)	−10.0(1)	5.0(2)	−1.2(2)
	0.7	−0.44(4)	−1.24(4)	3.1(2)	−6.4(1)		0.7	−1.28(1)	−12.5(1)	6.8(3)	−2.5(3)
1.25	0.3	−0.26(2)	−0.47(2)	0.34(2)	−0.81(4)	2.25	0.3	−0.43(4)	−7.0(1)	3.1(2)	0.2(2)
	0.4	−0.40(3)	−0.84(3)	0.69(3)	−1.34(5)		0.4	−0.59(5)	−9.7(1)	4.4(2)	−0.1(2)
	0.5	−0.54(4)	−1.31(4)	1.23(6)	−2.1(1)		0.5	−0.8(1)	−12.2(1)	5.6(3)	0.0(3)
	0.6	−0.67(5)	−1.91(5)	2.1(1)	−3.5(1)		0.6	−1.1(1)	−15.0(1)	7.0(4)	−0.2(4)
	0.7	−0.78(5)	−2.6(1)	3.5(2)	−5.8(1)		0.7	−1.26(3)	−18.2(2)	9.1(5)	−1.4(5)
1.50	0.3	−0.45(3)	−1.01(3)	0.50(3)	−0.59(5)	2.50	0.3	−0.32(3)	−10.3(1)	4.3(2)	1.1(2)
	0.4	−0.66(4)	−1.69(5)	0.98(5)	−1.1(1)		0.4	−0.54(4)	−13.8(1)	6.3(3)	0.4(3)
	0.5	−0.83(5)	−2.55(5)	1.6(1)	−1.7(1)		0.5	−0.76(5)	−17.2(1)	7.6(4)	1.0(4)
	0.6	−1.0(1)	−3.6(1)	2.6(1)	−2.8(2)		0.6	−1.0(1)	−20.8(1)	9.4(5)	0.8(5)
	0.7	−1.07(1)	−4.9(1)	4.1(2)	−4.7(2)		0.7	−1.5(1)	−24.9(1)	12.1(5)	−0.7(5)
1.75	0.3	−0.62(4)	−2.05(5)	0.85(4)	−0.3(1)						
	0.4	−0.83(5)	−3.3(1)	1.6(1)	−0.7(2)						
	0.5	−1.0(1)	−4.6(1)	2.4(1)	−1.2(2)						
	0.6	−1.1(1)	−6.2(1)	3.5(2)	−2.0(3)						
	0.7	−1.23(5)	−8.1(1)	5.2(3)	−3.7(3)						

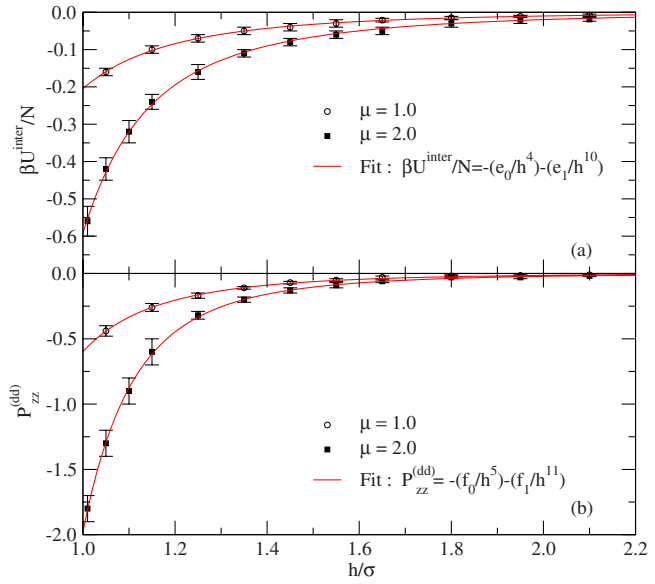

FIG. 2. (Color online) Average energies (a) and normal pressures (b) as functions of h for $\rho=0.7$ and $\mu=1$ and 2. The symbols denote MC data and the lines are fits to the data using Eqs. (21) and (22), respectively. The fitting parameters for $\mu=1$ are $e_0=0.16\pm0.01$, $e_1=0.045\pm0.002$ and $f_0=0.46\pm0.01$, $f_1=0.13\pm0.01$. For $\mu=2$ they are $e_0=0.31\pm0.01$, $e_1=0,28\pm0.01$ and $f_0=0.68\pm0.03$, $f_1=1.3\pm0.1$.

The effect is most pronounced at the lower density $\rho=0.3$.

The knowledge of $h^{112}_{\text{intra}}(s)$ and $h^{112}_{\text{inter}}(s)$ enables us to recover intralayer and interlayer energies according to

$$\frac{\beta\bar{U}^{\text{intra}}}{N}=-\frac{2\pi}{3}\beta\mu^2\rho\int_0^\infty\frac{1}{s^2}h^{112}_{\text{intra}}(s)ds,$$

$$\frac{\beta\bar{U}^{\text{inter}}}{N}=-\frac{2\pi}{3}\beta\mu^2\rho\int_0^\infty\frac{s}{(s^2+h^2)^{3/2}}h^{112}_{\text{inter}}(s)ds. \quad (26)$$

Similarly, the pressure tensor components are given by

$$\bar{P}^{(dd)}_{zz}=-4\pi\mu^2\rho^2h\int_0^\infty\frac{s}{(s^2+h^2)^{5/2}}h^{112}_{\text{inter}}(s)ds,$$

$$\bar{\Pi}^{(dd)}_T=-2\pi\mu^2\rho^2\left(\int_0^\infty\frac{1}{s^2}h^{112}_{\text{intra}}(s)ds+\int_0^\infty\frac{s^3}{(s^2+h^2)^{5/2}}h^{112}_{\text{inter}}(s)ds\right). \quad (27)$$

The quantities $\bar{U}^{\text{intra}}$, $\bar{U}^{\text{inter}}$, $\bar{P}^{(dd)}_{zz}$, and $\bar{\Pi}^{(dd)}_T$ computed with the functions $h^{112}_{\text{intra}}(s)$ and $h^{112}_{\text{inter}}(s)$ can serve as a consistency check with the direct simulation results for energy and pressure using Ewald summations (Tables III and IV). Such a comparison is, however, conclusive only if the correlation functions decay to zero on the scale of the simulation box which was fulfilled only at the lower μ values (cf. Figures 4–6 for the correlation functions). For example, at $h=1.05$, $\rho=0.7$, and $\mu=1.0$ one has $\beta\bar{U}^{\text{intra}}/N=-0.55$, $\beta\bar{U}^{\text{inter}}/N=-0.16$, $\bar{P}^{(dd)}_{zz}=-0.43$, and $\bar{\Pi}^{(dd)}_T=-1.26$ in good agreement with the results of Tables III and IV. For $h=1.05$, $\rho=0.7$, and $\mu=2.0$, integrating up to half the box length, one has $\beta\bar{U}^{\text{intra}}/N=-5.9$, $\beta\bar{U}^{\text{inter}}/N=-0.42$, $\bar{P}^{(dd)}_{zz}=-1.40$, and $\bar{\Pi}^{(dd)}_T=-12.6$, which compare favorably with the values of Tables III and IV.

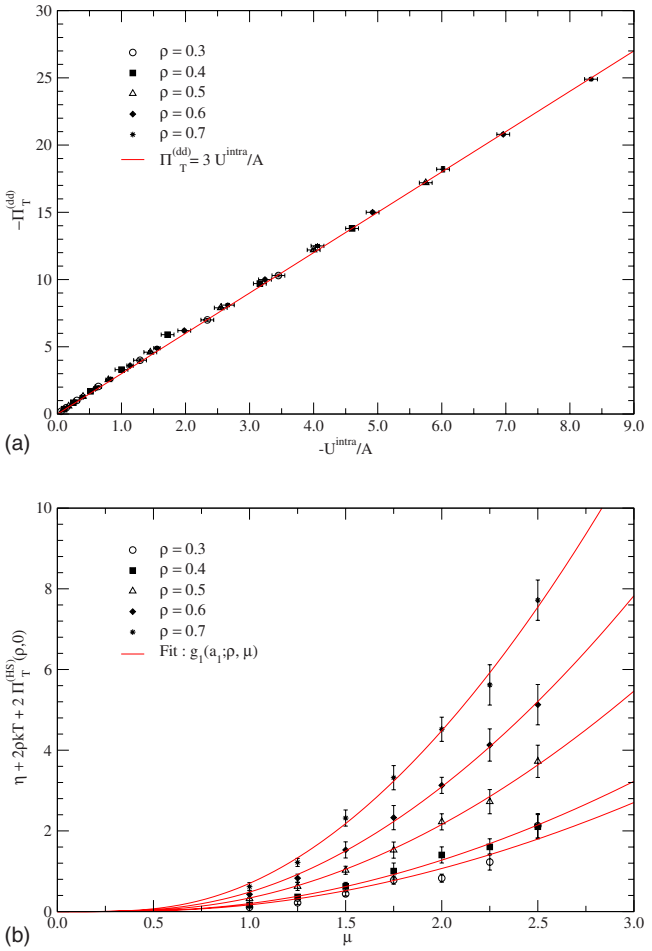

FIG. 3. (Color online) (a) Lateral pressure as a function of the intralayer energy per unit area. Symbols are data from Tables III and IV for densities $\rho=0.3-0.7$, dipole strengths $\mu=1.0-2.5$, and $h=1.05$; the straight line is given by Eq. (23). (b) Surface stress as function of dipole strength for $\rho=0.3-0.7$ and $h=1.05$. Symbols are data from Table IV and lines are given by Eq. (25) with $g_1(a_1;\rho,\mu)=a_1\rho^2\mu^4/(1+\mu^2)$ ($a_1\sim2.7$) and $\Pi^{(\text{HS})}_T(\rho,0)$ given by the equation of state of hard disks [27].

Equations (26) and (27), show that we have the relation $\bar{\Pi}^{(dd)}_T=3\bar{U}^{\text{intra}}/A$ for $h\to\infty$; this asymptotic behavior is in accordance with Eq. (23). However, it is surprising that Eq. (23) is verified with such accuracy even for $h=1.05$ [see Sec. IV C and Fig. 3(a)].

The values of h^{220} for $s\gtrsim7$ agree well with Eq. (18). For example, at $\mu=2.5$ on has $P_2\sim0.42$ for both densities 0.3 and 0.7. This low value of P_2 merely indicates some prevalent local nematic ordering but no global long-range nematic ordering of the dipole moments.

The characterization of the structural organization of the particles in the bilayer at high densities is subject to greater

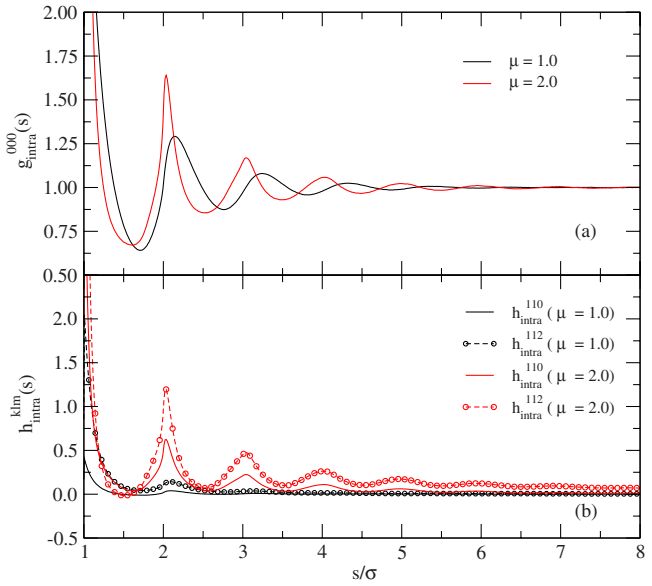

FIG. 4. (Color online) Intralayer angle-averaged pair distribution function (a) $g^{000}_{\text{intra}}(s)$ and angular projections (b) $h^{klm}_{\text{intra}}(s)$ for a bilayer of dipolar hard spheres at $\rho=0.7$, $h=1.05$, for $\mu=1.0$ (black) and 2.0 [red (gray)].

uncertainty due to system size dependence and convergence problems. To illustrate the difficulties we refer to snapshots of configurations at $\rho=0.9$, $\mu=2$, and $h=1.05$ taken at different "time" intervals during the MC evolution of the system shown in Figs. 8(a)–8(d). The system, with 2×1600 particles, was started from two square lattices with random orientations of the dipole moments. Already after 500 cycles of trial moves small vortices have built up, predominantly around particles with dipole moments oriented perpendicularly to the layers [Fig. 8(a)]. As sampling proceeds, the vortices grow bigger and large patches develop within which particles arrange with local hexagonal order and parallel alignement of the dipole moments [Figs. 8(b) and 8(c)], clearly an energetically favorable ordering. It remains somewhat unclear whether, for small system sizes, the PBCs can stabilize such a ferroelectric arrangement. Such a possibility was indeed observed for a smaller system size (2×576 particles) [see Figure 8(d)], and in one instance ($h=1.005$, $\mu=2$) also for the 2×1600 system though an independent run of similar length (1×10^6 cycles) at the same state point retained a vortex arrangement. In some cases, for the smaller 2×576 system, we also observed formation of stripes with opposite directions of the dipole moments.

The structural behavior just described seems typical for dipole strength $\mu\sim2$ and does not depend much on layer separation in the range $h=1-2$. For larger dipole moments the vortex structure appears to be more stable but, evidently, relaxation of the dipole moments is also slower. Certainly there are strong structural correlations between the layers. As for the lower densities, particles arrange preferentially to sit on top of each other with opposite directions of the dipole moments.

Finally, in Fig. 9 we show the organization of dipole moments in a bilayer with $h=1.05$ for close packed square and hexagonal lattices of the HSs (disks). In both cases the HSs in the two layers were taken to be on top of each other. On the square lattices ($\rho=1.0$) the dipole moments in each layer align in parallel lines along the box edges with opposite directions of the dipole moments in neighboring lines [Fig. 9(a)]. A small tendency of microvortex formation is observed. These arrangements are typical of (monolayer) ground state configurations. For a square lattice of in-plane dipoles, the ground state is continuously degenerated but thermal contributions can select configurations where rows or colums of parallel spins alternate [38]. In contrast, for the

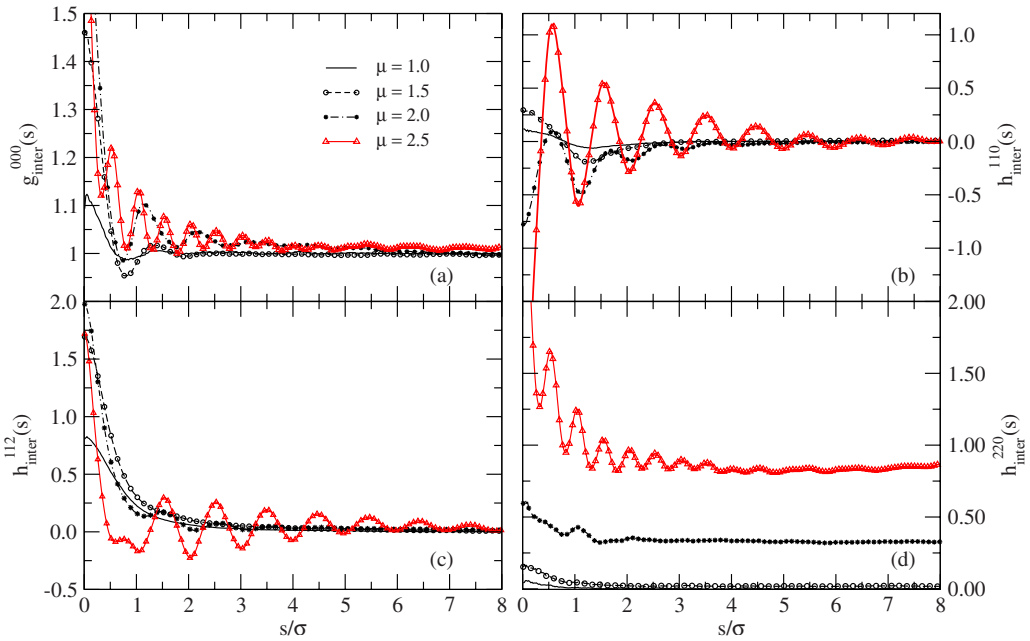

FIG. 5. (Color online) Interlayer angle-averaged pair distribution function $g^{000}_{\text{inter}}(s)$ and angular projections $h^{klm}_{\text{inter}}(s)$ of the pair distribution functions $g_{\text{inter}}(12)$ for the DHS bilayer at $\rho=0.3$ and $h=1.05$ for several values of μ. (a) $g^{000}_{\text{inter}}(s)$; (b) $h^{110}_{\text{inter}}(s)$; (c) $h^{112}_{\text{inter}}(s)$, (d) $h^{220}_{\text{inter}}(s)$.

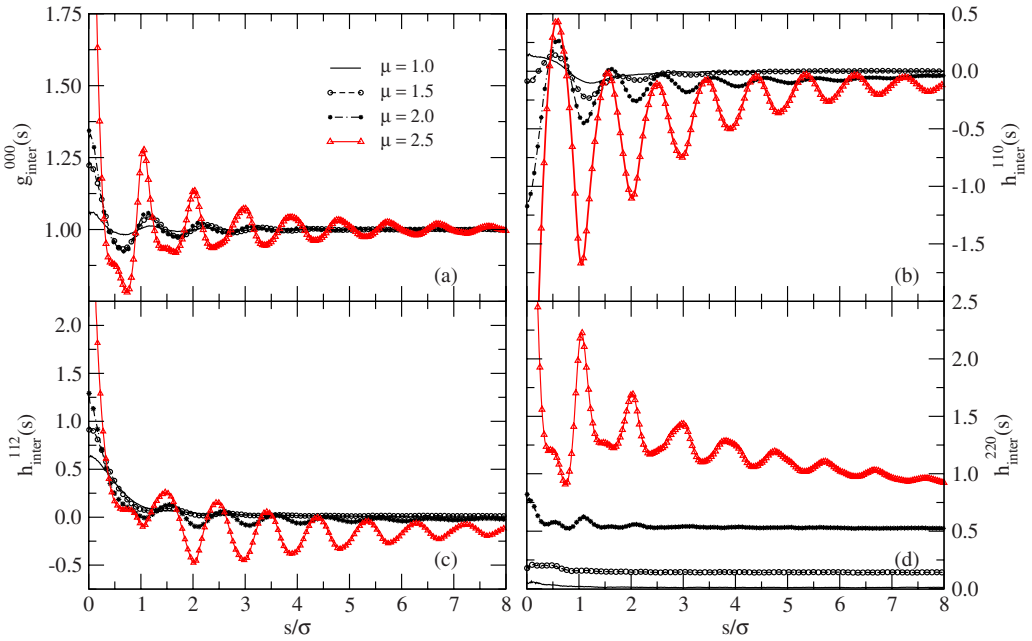

FIG. 6. (Color online) Same as Fig. 5 but for $\rho=0.7$.

2D triangular lattice with in-plane dipoles, the ground state of the infinite system is ferroelectric [39,40]; in finite systems the dipolar ordering in the ground state may, however, depend on the system size and aspect ratio of the lattice [41]. In the present finite-temperature calculations ($\rho=1.15$), we observe a ferroelectric phase with slight zigzag ordering of the dipole moments [Fig. 9(b)]. The influence on ordering of dipole strength, system size, and use of PBCs has still to be investigated. It should be noted also that in our calculations the dipoles are not completely in plane. As expected, for both lattices, dipole moments in different layers run in opposite directions.

V. SUMMARY AND CONCLUSION

We have investigated by MC simulation the structural and thermodynamic properties of fully orientable dipolar hard spheres mobile in two parallel planar surfaces with particular emphasis on the forces between the two layers. Interlayer correlations turn out to be quite small, almost vanishing at layer separations of two HS diameters. The interlayer energy is attractive for all states considered and the normal pressure is negative, meaning that an external force must be supplied to keep the layers apart. Indeed isobaric MC simulations, allowing h to fluctuate, did not enable us to find an equilibrium state; either the system collapsed (at low applied negative pressure) or the two layers drifted away (at larger pressures). The normal pressure is well described by a $-1/h^5$ dependence at larger separations in agreement with a second-order perturbation theory of the interaction free energy of the surfaces in an infinite dielectric medium by Attard and Mitchell [35,36]. Despite the weak interlayer energy there are strong correlations for the structural behavior of the particles in the two layers. Particles preferentially sit on top of each other with opposite orientations of the dipole moments. At densities of the order $\rho\sim 0.9$ convergence of the MC sampling is slow and, moreover, finite-size effects may affect the results. Although we believe that for large systems vortex formation is the preferred structure, arrangements with ferroelectric ordering or stripes with up and down orientations of the dipole moments were stabilized in the smaller systems, likely by the use of periodic boundary conditions. These problems clearly need a more detailed investigation.

As an extension of the present work it would be of interest to consider the case where the media on either side of the layers have different dielectric constants, as would be the case, for instance, in a lipid bilayer model where the hydrocarbon tails and aqueous regions are approximated by ideal dielectrics. Although the surface polarization arising from the dielectric discontinuities can in principle be taken into account through dielectric images [42], few simulation results have been presented so far [43]. Such simulations could valuably add to the comprehension of the origin of the repulsive "hydration" forces measured in phospholipid bilayers at short distances [44]. Existing theoretical approaches based on continuum electrostatics [36,45] seem to fail to predict correctly these repulsive forces.

ACKNOWLEDGMENTS

The computations have been performed on IBM Regatta Power 4 stations of IDRIS (Institut du Développement et des Ressources en Informatique Scientifique) under Projects No. 0672104 and No. 0682104. C.A. acknowledges financial support by COLCIENCIAS and SECAB (Executive Secretariat of the Andes Bello Convention) in the framework of the cooperation treaty 065-2002. The work has benefitted from support of the project ECOS-Nord CO5PO2.

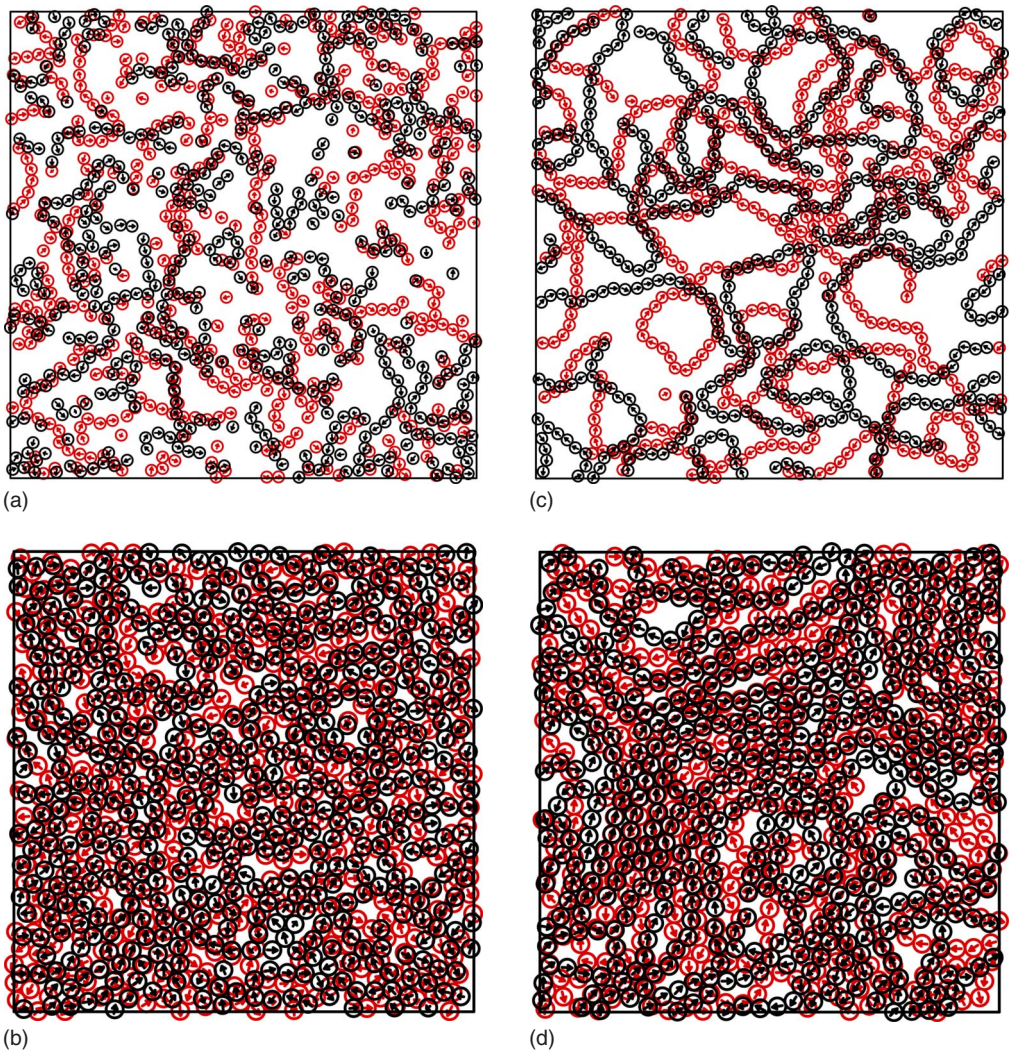

FIG. 7. (Color online) Snapshots of bilayer configurations of particles at $\mu=2.0$ (a),(b) and 2.50 (c),(d) for $h=1.05$; snapshots (a) and (c) are for $\rho=0.3$ ($N=1058$); snapshots (b) and (d) for $\rho=0.7$ ($N=1024$). Particles in different layers are represented by different colors. The HS cores are represented by circles of diameter $\sigma=1$ and the directions of dipole moments by arrows.

APPENDIX A: EWALD SUMS FOR THE DIPOLAR ENERGY OF THE BILAYER

The total dipolar energy of the bilayer computed with the Ewald method is written as

$$U_{dd} = E_{\boldsymbol{r}} + E^{(1)}_{\boldsymbol{G}\neq 0} + E^{(2)}_{\boldsymbol{G}\neq 0} + E^{(3)}_{\boldsymbol{G}\neq 0} + E_{\boldsymbol{G}=0}. \tag{A1}$$

Here $E_{\boldsymbol{r}}$ is the short-range (direct space) contribution to the energy given by

$$E_{\boldsymbol{r}} = \frac{1}{2}\sum_{i\neq j}\left[(\boldsymbol{\mu}_i\cdot\boldsymbol{\mu}_j)B(r_{ij}) - (\boldsymbol{\mu}_i\cdot\boldsymbol{r}_{ij})(\boldsymbol{\mu}_j\cdot\boldsymbol{r}_{ij})C(r_{ij})\right] \tag{A2}$$

with

$$B(r) = \frac{\operatorname{erfc}(\alpha r)}{r^3} + \frac{2\alpha}{\sqrt{\pi}}\frac{\exp(-\alpha^2 r^2)}{r^2},$$

$$C(r) = 3\frac{\operatorname{erfc}(\alpha r)}{r^5} + \frac{2\alpha}{\sqrt{\pi}}\left(2\alpha^2 + \frac{3}{r^2}\right)\frac{\exp(-\alpha^2 r^2)}{r^2}. \tag{A3}$$

In Eq. (A2) it is assumed that the parameter α is sufficiently large to restrict interactions to the basic simulation cell. The energy $E_{\boldsymbol{r}}$ can, in turn, be separated into an intralayer, $E^{\text{intra}}_{\boldsymbol{r}}$, and an interlayer, $E^{\text{inter}}_{\boldsymbol{r}}$, contribution. The four last terms in Eq. (A1) are the reciprocal space contributions. Each of the terms is again separated into intralayer and interlayer contributions. They are split into three contributions: $E^{(1)}_{\boldsymbol{G}\neq 0}$ involves only coupling between the normal components of dipole moments, $E^{(2)}_{\boldsymbol{G}\neq 0}$ coupling between in-plane and normal components of dipoles, and $E^{(3)}_{\boldsymbol{G}\neq 0}$ in-plane coupling. Contributions to the interlayer energy are given by

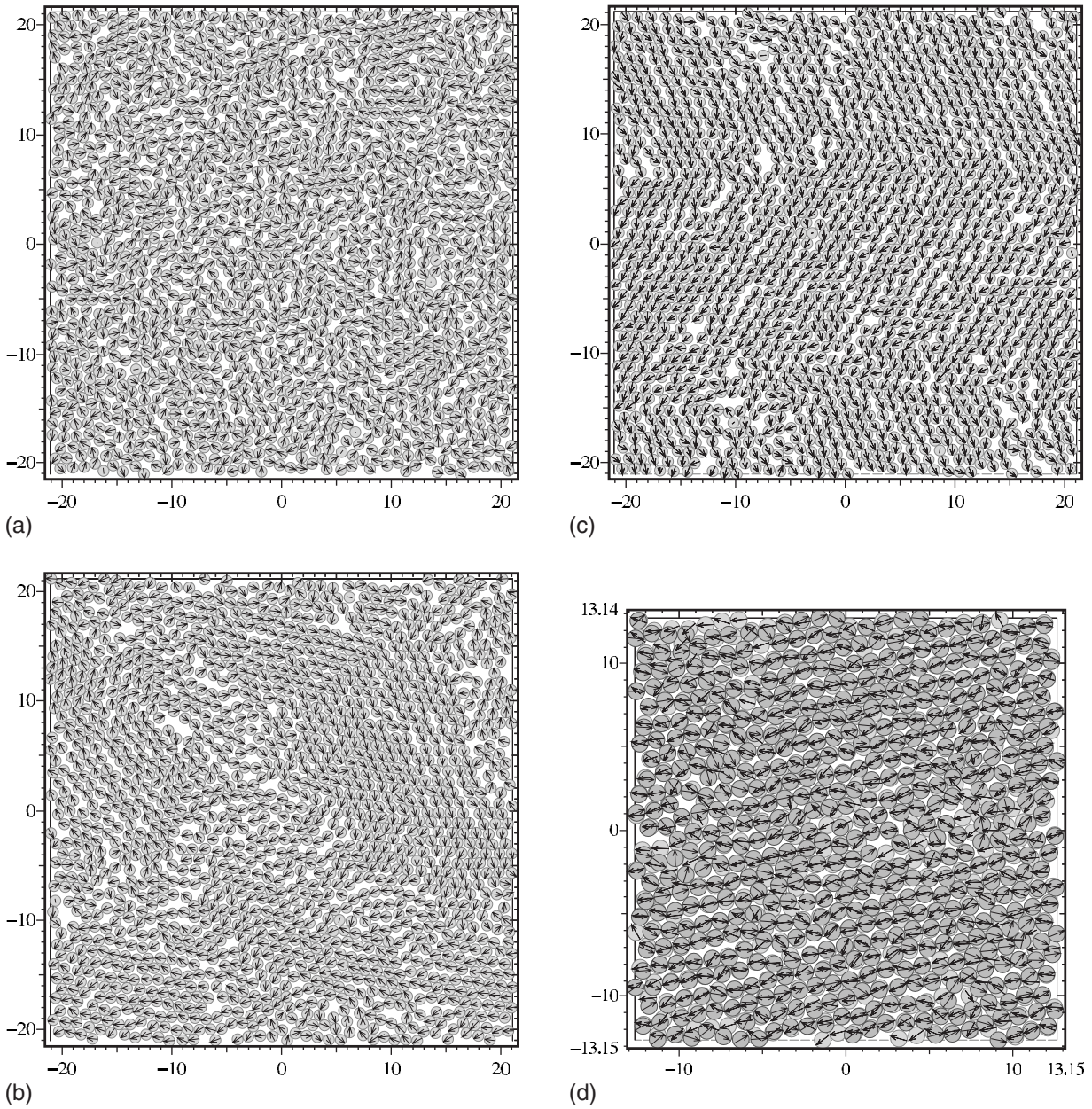

FIG. 8. Bilayer configurations of the 2×1600 particle system at $\rho=0.9$, $\mu=2$, and $h=1.05$ at different intervals of the MC simulation; snapshot after (a) 500 cycles, (b) 0.26×10^6 cycles, and (c) 1.75×10^6 cycles. (d) Result for 2×576 particles after 2.6×10^6 cycles. For clarity only the particle arrangements in one layer are shown in (a)–(c). The arrows denote the projections of the dipole moments on the layer plane. Thus dipoles perpendicular to the layer appear as dots.

$$E_{\boldsymbol{G}\neq0}^{(1,\mathrm{inter})}=\frac{\pi}{A}\sum_{\boldsymbol{G}\neq0}I(\alpha,G;h)\mathrm{Re}\left[\left(\sum_{i\in L_1}\mu_i^z\exp(i\boldsymbol{G}\cdot\boldsymbol{s}_i)\right)\times\left(\sum_{j\in L_2}\mu_j^z\exp(-i\boldsymbol{G}\cdot\boldsymbol{s}_j)\right)\right],$$

$$E_{\boldsymbol{G}\neq0}^{(2,\mathrm{inter})}=\frac{\pi}{A}\sum_{\boldsymbol{G}\neq0}J(\alpha,G;h)\mathrm{Im}\left[\left(\sum_{i\in L_1}(\boldsymbol{\mu}_i\cdot\boldsymbol{G})\exp(i\boldsymbol{G}\cdot\boldsymbol{s}_i)\right)\times\left(\sum_{j\in L_2}\mu_j^z\exp(-i\boldsymbol{G}\cdot\boldsymbol{s}_j)\right)+\left(\sum_{i\in L_1}\mu_i^z\exp(i\boldsymbol{G}\cdot\boldsymbol{s}_i)\right)\times\left(\sum_{j\in L_2}(\boldsymbol{\mu}_j\cdot\boldsymbol{G})\exp(-i\boldsymbol{G}\cdot\boldsymbol{s}_j)\right)\right],$$

$$E_{\boldsymbol{G}\neq0}^{(3,\mathrm{inter})}=\frac{\pi}{A}\sum_{\boldsymbol{G}\neq\boldsymbol{0}}K(\alpha,G;h)\mathrm{Re}\left[\left(\sum_{i\in L_1}(\boldsymbol{\mu}_i\cdot\boldsymbol{G})\exp(i\boldsymbol{G}\cdot\boldsymbol{s}_i)\right)\times\left(\sum_{j\in L_2}(\boldsymbol{\mu}_j\cdot\boldsymbol{G})\exp(-i\boldsymbol{G}\cdot\boldsymbol{s}_j)\right)\right],\tag{A4}$$

where $\mathrm{Re}[z]$ and $\mathrm{Im}[z]$ are the real and imaginary parts of the complex number z, respectively. $\boldsymbol{G}=2\pi(\frac{n_x}{L_x},\frac{n_y}{L_y})$, ($n_x$, n_y integers) is a two-dimensional vector in the reciprocal lattice and $G=\|\boldsymbol{G}\|$. The functions $I(\alpha,G;h)$, $J(\alpha,G;h)$, and $K(\alpha,G;h)$ are given by

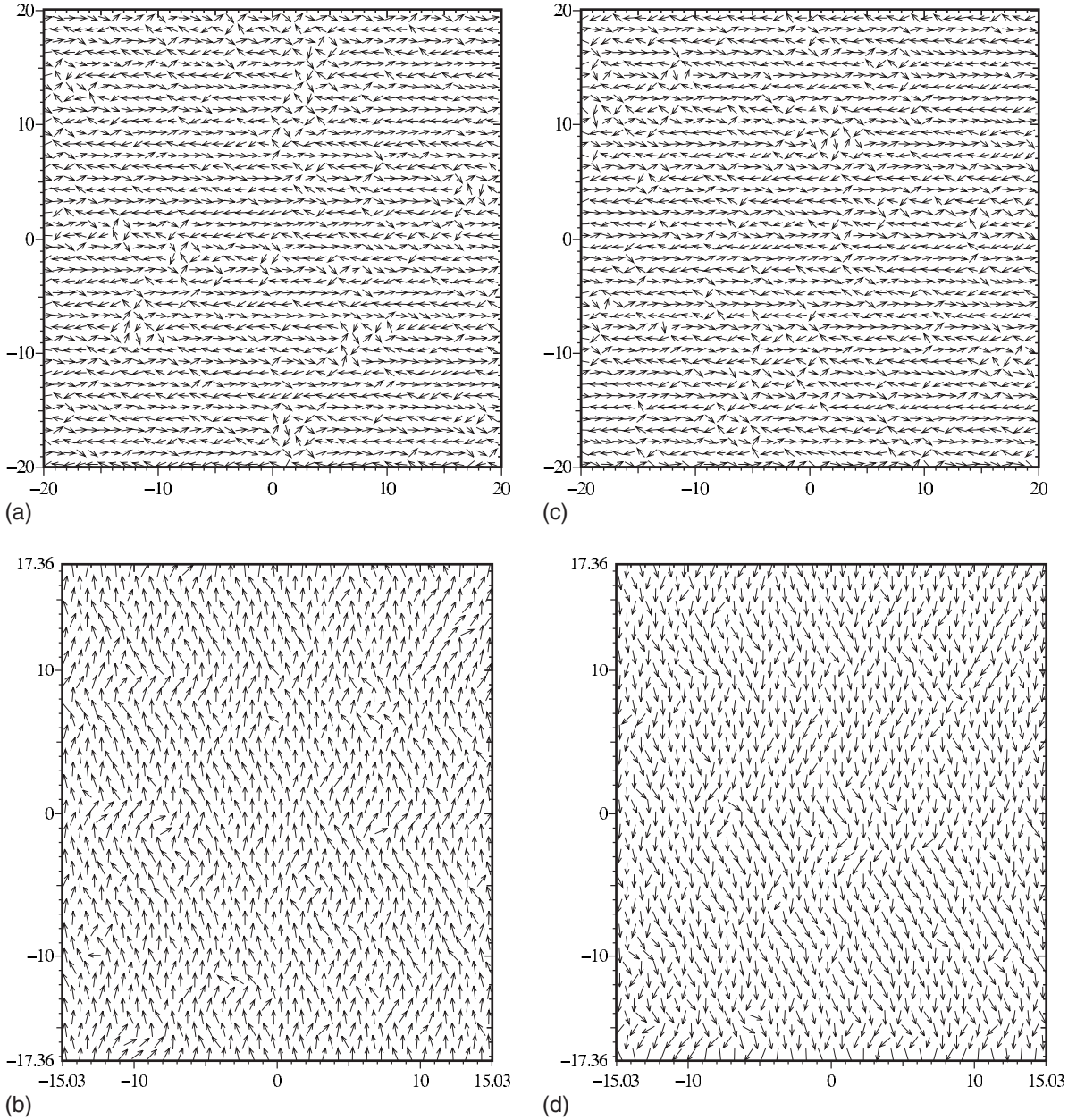

FIG. 9. Snapshots of bilayer configurations of particles at close packing. (a) square lattice ($\rho=1$, $\mu=2$, $h=1.05$, N=3200); (b) hexagonal lattice ($\rho=1.15$, $\mu=2$, $h=1.05$, N=2400). The particles in the two layers are on top of each other. The arrows denote the projections of the dipole moments on the layer plane. The two layers are shown separately.

$$I(\alpha,G;h)=\frac{4\alpha}{\sqrt{\pi}}\exp\left(-\frac{G^2}{4\alpha^2}-\alpha^2h^2\right)-G^2K(\alpha,G;h),$$

$$J(\alpha,G;h)=\exp(Gh)\mathrm{erfc}\left(\frac{G}{2\alpha}+\alpha h\right)-\exp(-Gh)\mathrm{erfc}\left(\frac{G}{2\alpha}-\alpha h\right),$$

$$K(\alpha,G;h)=\frac{1}{G}\left[\exp(Gh)\mathrm{erfc}\left(\frac{G}{2\alpha}+\alpha h\right)+\exp(-Gh)\mathrm{erfc}\left(\frac{G}{2\alpha}-\alpha h\right)\right]. \quad \text{(A5)}$$

The constant term is

$$E^{(\mathrm{inter})}_{G=0}=\frac{4\alpha\sqrt{\pi}}{A}\exp(-\alpha^2h^2)\left[\left(\sum_{i\in L_1}\mu_i^z\right)\left(\sum_{j\in L_2}\mu_j^z\right)\right]. \quad \text{(A6)}$$

Contributions to the intralayer energy are given by

$$E_{\boldsymbol{G}\neq 0}^{(1,\mathrm{intra})} = \frac{\pi}{A}\sum_{\boldsymbol{G}\neq 0} D(\alpha,G)\left(\left|\sum_{i\in L_1}\mu_i^z \exp(i\boldsymbol{G}\cdot\boldsymbol{s}_i)\right|^2 + \left|\sum_{j\in L_2}\mu_j^z \exp(i\mathbf{G}\cdot\mathbf{s}_j)\right|^2\right),$$

$$E_{\boldsymbol{G}\neq 0}^{(2,\mathrm{intra})} = 0,$$

$$E_{\boldsymbol{G}\neq 0}^{(3,\mathrm{intra})} = \frac{\pi}{A}\sum_{\boldsymbol{G}\neq 0} H(\alpha,G)\left(\left|\sum_{i\in L_1}(\boldsymbol{\mu}_i\cdot\boldsymbol{G})\exp(i\boldsymbol{G}\cdot\boldsymbol{s}_i)\right|^2 + \left|\sum_{j\in L_2}(\boldsymbol{\mu}_j\cdot\boldsymbol{G})\exp(i\boldsymbol{G}\cdot\boldsymbol{s}_j)\right|^2\right), \tag{A7}$$

with

$$D(\alpha,G) = \frac{2\alpha}{\sqrt{\pi}}\exp(-G^2/4\alpha^2) - G\,\mathrm{erfc}(G/2\alpha),$$

$$H(\alpha,G) = \frac{\mathrm{erfc}(G/2\alpha)}{G}, \tag{A8}$$

and the constant is

$$E_{\boldsymbol{G}=0}^{(\mathrm{intra})} = \frac{2\alpha\sqrt{\pi}}{A}\left[\left(\sum_{i\in L_1}\mu_i^z\right)^2 + \left(\sum_{j\in L_2}\mu_j^z\right)^2\right] - \frac{2\alpha^3}{3\sqrt{\pi}}\sum_i \boldsymbol{\mu}_i^2. \tag{A9}$$

Due to the 2D character of $\boldsymbol{G}$ it is easily seen from the corresponding term in Eq. (A4) (interlayer contribution) that $E_{\boldsymbol{G}\neq 0}^{(2,\mathrm{intra})}$ must vanish.

APPENDIX B: THE MICROSCOPIC STRESS TENSOR OF THE BILAYER

In this appendix, we derive the microscopic stress tensor for the bilayer system from its equations of motion, in a way similar to the one of Ref. [[28](a)] for inhomogeneous fluids. The microscopic stress tensor of the bilayer is split into normal σ_N and lateral σ_T components as

$$\sigma = \sigma_T + \sigma_N = \begin{pmatrix} \sigma_{xx} & \sigma_{xy} & 0 \\ \sigma_{xy} & \sigma_{yy} & 0 \\ 0 & 0 & 0 \end{pmatrix} + \begin{pmatrix} 0 & 0 & \sigma_{xz} \\ 0 & 0 & \sigma_{yz} \\ \sigma_{xz} & \sigma_{yz} & \sigma_{zz} \end{pmatrix}. \tag{B1}$$

The Lagrangian function of the bilayer system, with the constraints $z_i=H_1$ for $i\in L_1$, and $z_i=H_2$ for $i\in L_2$ is given by

$$\mathcal{L} = \sum_{i\in L_1\cup L_2}\frac{1}{2}m_i\dot{\boldsymbol{s}}_i^2 + \sum_{i\in L_1}\frac{1}{2}m_i\dot{H}_1^2 + \sum_{i\in L_2}\frac{1}{2}m_i\dot{H}_2^2 - \frac{1}{2}\sum_i\sum_{j\neq i}\Phi(\boldsymbol{s}_{ij},z_{ij}) - \sum_{i\in L_1\cup L_2}\Phi_{\mathrm{ext}}(\boldsymbol{s}_i,z_i), \tag{B2}$$

where Φ is the pair potential energy due to interactions between particles and Φ_{ext} represents the action of any external fields. In the above equation, H_1 and H_2 are collective variables associated with the z coordinate of the layers. From the Lagrangian of the system, we obtain the equations of motion for the particles in the layer L_1 and the collective variable H_1:

$$m\ddot{\boldsymbol{s}}_i = -\sum_{j\in L_1, j\neq i}\boldsymbol{\nabla}_i\Phi(\mathbf{s}_{ij},0) - \sum_{j\in L_2}\boldsymbol{\nabla}_i\Phi(\boldsymbol{s}_{ij},H_2-H_1) - \boldsymbol{\nabla}_i\Phi_{\mathrm{ext}}(\boldsymbol{s}_i,H_1), \tag{B3}$$

$$N_0 m\ddot{H}_1 = \frac{\partial}{\partial z}\sum_{i\in L_1}\sum_{j\in L_2}\Phi(\boldsymbol{s}_{ij},H_2-H_1) - \frac{\partial}{\partial z}\sum_{i\in L_1}\Phi_{\mathrm{ext}}(\boldsymbol{s}_i,H_1), \tag{B4}$$

and similar equations for the layer L_2. m denotes the mass of the particles.

The momentum density for the bilayer system can be written as

$$\boldsymbol{J}(\boldsymbol{s},z,t) = \boldsymbol{J}_T(\boldsymbol{s},z,t) + J_N(\boldsymbol{s},z,t)\hat{\boldsymbol{e}}_z = m\delta(z-H_1)\sum_{i\in L_1}\dot{\boldsymbol{s}}_i\delta(\boldsymbol{s}-\boldsymbol{s}_i) + m\delta(z-H_2)\sum_{i\in L_2}\dot{\boldsymbol{s}}_i\delta(\boldsymbol{s}-\boldsymbol{s}_i) + m\dot{H}_1\delta(z-H_1)\times\sum_{i\in L_1}\delta(\boldsymbol{s}-\boldsymbol{s}_i)\hat{\boldsymbol{e}}_z + m\dot{H}_2\delta(z-H_2)\sum_{i\in L_2}\delta(\boldsymbol{s}-\boldsymbol{s}_i)\hat{\boldsymbol{e}}_z, \tag{B5}$$

where $\delta(x)$ is the Dirac distribution. From the time derivative of the momentum density, we obtain easily [28] the kinetic contribution to the lateral component of the stress tensor as

$$\sigma_{\alpha\beta}^K(\boldsymbol{s},z,t) = -m\delta(z-H_1)\sum_{i\in L_1}\dot{\boldsymbol{s}}_i^\alpha\dot{\boldsymbol{s}}_i^\beta\delta(\boldsymbol{s}-\boldsymbol{s}_i) - m\delta(z-H_2)\sum_{i\in L_2}\dot{\boldsymbol{s}}_i^\alpha\dot{\boldsymbol{s}}_i^\beta\delta(\boldsymbol{s}-\boldsymbol{s}_i) \tag{B6}$$

with $\alpha,\beta=x,y$. The kinetic contribution to the normal component is obtained similarly as

$$\sigma_{\alpha z}^K(\boldsymbol{s},z,t) = -m\dot{H}_1\delta(z-H_1)\sum_{i\in L_1}\dot{\boldsymbol{s}}_i^\alpha\delta(\boldsymbol{s}-\boldsymbol{s}_i) - m\dot{H}_2\delta(z-H_2)\sum_{i\in L_2}\dot{\boldsymbol{s}}_i^\alpha\delta(\boldsymbol{s}-\boldsymbol{s}_i),$$

$$\sigma_{zz}^K(\boldsymbol{s},z,t) = -m\dot{H}_1^2\delta(z-H_1)\sum_{i\in L_1}\delta(\boldsymbol{s}-\boldsymbol{s}_i) - m\dot{H}_2^2\delta(z-H_2)\sum_{i\in L_2}\delta(\boldsymbol{s}-\boldsymbol{s}_i). \tag{B7}$$

The configurational contributions to the stress tensor, follow from Eq. (B3),

$$\sigma^C_{\alpha\beta}(\boldsymbol{s},z,t)=\left(\frac{1}{2}\sum_{i\in L_1}\sum_{j\in L_1,j\neq i}\nabla^\alpha_i\Phi(\boldsymbol{s}_{ij},0)\int_{C_{ij}}dl^\beta\,\delta(\boldsymbol{s}-\boldsymbol{l})+\frac{1}{2}\sum_{i\in L_1}\sum_{j\in L_2}\nabla^\alpha_i\Phi(\boldsymbol{s}_{ij},H_2-H_1)\int_{C_{ij}}dl^\beta\,\delta(\boldsymbol{s}-\boldsymbol{l})\right)\delta(z-H_1)$$
$$+\left(\frac{1}{2}\sum_{i\in L_2}\sum_{j\in L_2,j\neq i}\nabla^\alpha_i\Phi(\boldsymbol{s}_{ij},0)\int_{C_{ij}}dl^\beta\,\delta(\boldsymbol{s}-\boldsymbol{l})+\frac{1}{2}\sum_{i\in L_2}\sum_{j\in L_1}\nabla^\alpha_i\Phi(\boldsymbol{s}_{ij},H_1-H_2)\int_{C_{ij}}dl^\beta\,\delta(\boldsymbol{s}-\boldsymbol{l})\right)\delta(z-H_2) \quad \text{(B8)}$$

with $\alpha=x,y$ and C_{ij} a contour joining $\boldsymbol{s}_i$ to $\boldsymbol{s}_j$ in the plane perpendicular to the z direction. Equations (B8) and (B6) allow one to fully determine the lateral component of the stress tensor of the bilayer. The integrals in Eq. (B8) can be evaluated by using the parametrization proposed by Irving and Kirkwood [[28](b)], namely,

$$\sum_{i\in L_1}\sum_{j\in L_1,j\neq i}\nabla^\alpha_i\Phi(\boldsymbol{s}_{ij},0)\int_{C_{ij}}dl^\beta\,\delta(\boldsymbol{s}-\boldsymbol{l})$$
$$=\sum_{i\in L_1}\sum_{j\in L_1,j\neq i}s^\beta_{ij}\nabla^\alpha_i\Phi(\boldsymbol{s}_{ij},0)\int_0^1 d\lambda\;\delta(\boldsymbol{s}-\lambda\boldsymbol{s}_j-(1-\lambda)\boldsymbol{s}_i) \quad \text{(B9)}$$

and

$$\sum_{i\in L_1}\sum_{j\in L_2}\nabla^\alpha_i\Phi(\boldsymbol{s}_{ij},H_2-H_1)\int_{C_{ij}}dl^\beta\,\delta(\boldsymbol{s}-\boldsymbol{l})$$
$$=\sum_{i\in L_1}\sum_{j\in L_2}s^\beta_{ij}\nabla^\alpha_i\Phi(\boldsymbol{s}_{ij},H_2-H_1)\times\int_0^1 d\lambda\;\delta(\boldsymbol{s}-\lambda\boldsymbol{s}_j-(1-\lambda)\boldsymbol{s}_i)$$
$$=\sum_{i\in L_2}\sum_{j\in L_1}s^\beta_{ij}\nabla^\alpha_i\Phi(\boldsymbol{s}_{ij},H_1-H_2)\times\int_0^1 d\lambda\;\delta(\boldsymbol{s}-\lambda\boldsymbol{s}_j-(1-\lambda)\boldsymbol{s}_i). \quad \text{(B10)}$$

Equations (B6) and (B8) show that $\sigma_{\alpha\beta}$ can be written in the form $(\alpha,\beta=x,y)$

$$\sigma_{\alpha\beta}(\boldsymbol{s},z,t)=\tau^{(1)}_{\alpha\beta}(\boldsymbol{s},t)\,\delta(z-H_1)+\tau^{(2)}_{\alpha\beta}(\boldsymbol{s},t)\,\delta(z-H_2). \quad \text{(B11)}$$

One should note that, if $z\neq H_1$ and $z\neq H_2$, then $\sigma_{\alpha\beta}(\boldsymbol{s},z,t)=0$.

In accord with solid surface physics, we define the surface stress tensor as

$$\eta_{\alpha\beta}(\boldsymbol{s},t)=\int\sigma_{\alpha\beta}(\boldsymbol{s},z,t)dz=\tau^{(1)}_{\alpha\beta}(\boldsymbol{s},t)+\tau^{(2)}_{\alpha\beta}(\boldsymbol{s},t). \quad \text{(B12)}$$

If one adopts the two-component monolayer picture discussed in the main text, then the two contributions $\tau^{(1)}_{\alpha\beta}$ and $\tau^{(2)}_{\alpha\beta}$ correspond, respectively, to the partial contribution of each species to the surface stress tensor.

From the surface stress tensor we define the lateral component of the pressure tensor of the bilayer as the ensemble average of the surface stress tensor as

$$\Pi_{\alpha\beta}=-\left\langle\frac{1}{A}\int_{L_1\cup L_2}ds\;\eta_{\alpha\beta}(\boldsymbol{s},t)\right\rangle. \quad \text{(B13)}$$

It follows that

$$\Pi_{\alpha\beta}=2\rho kT\delta_{\alpha\beta}-\left\langle\frac{1}{2A}\sum_{i\in L_1}\sum_{j\in L_1,j\neq i}s^\beta_{ij}\nabla^\alpha_i\Phi(\boldsymbol{s}_{ij},0)\right\rangle$$
$$-\left\langle\frac{1}{2A}\sum_{i\in L_2}\sum_{j\in L_2,j\neq i}s^\beta_{ij}\nabla^\alpha_i\Phi(\boldsymbol{s}_{ij},0)\right\rangle$$
$$-\left\langle\frac{1}{A}\sum_{i\in L_1}\sum_{j\in L_2}s^\beta_{ij}\nabla^\alpha_i\Phi(\boldsymbol{s}_{ij},H_2-H_1)\right\rangle. \quad \text{(B14)}$$

The average lateral pressure Π_T and the surface stress $\tilde{\eta}$ are then given by

$$\Pi_T=\frac{1}{2}(\Pi_{xx}+\Pi_{yy})=-\tilde{\eta}. \quad \text{(B15)}$$

The configurational contribution to the normal component σ_{zz} allows us to obtain the force acting on the layers. From the equations of motion of H_1 and H_2, we obtain

$$\frac{\partial}{\partial z}\sigma^C_{zz}(\boldsymbol{s},z,t)=\frac{1}{N_0}\left(\sum_{n\in L_1}\delta(\boldsymbol{s}-\boldsymbol{s}_n)\right)\delta(z-H_1)\times\left(\frac{\partial}{\partial z}\sum_{i\in L_1}\sum_{j\in L_2}\Phi(\boldsymbol{s}_{ij},z)|_{z=H_2-H_1}\right)$$
$$-\frac{1}{N_0}\left(\sum_{n\in L_2}\delta(\boldsymbol{s}-\boldsymbol{s}_n)\right)\delta(z-H_2)\times\left(\frac{\partial}{\partial z}\sum_{i\in L_1}\sum_{j\in L_2}\Phi(\boldsymbol{s}_{ij},z)|_{z=H_2-H_1}\right). \quad \text{(B16)}$$

Thus, the total force $F^z_{2\to1}$ acting on layer L_1 due to the particles in layer L_2 is given by

$$F^z_{2\to1}=-\int ds\frac{\partial}{\partial z}\sigma^C_{zz}(\boldsymbol{s},z=H_1,t)$$
$$=-\frac{\partial}{\partial z}\sum_{i\in L_1}\sum_{j\in L_2}\Phi(\boldsymbol{s}_{ij},z)|_{z=H_2-H_1}, \quad \text{(B17)}$$

and, obviously, we have

$$F^z_{1\to 2} = -\int ds \frac{\partial}{\partial z}\sigma^C_{zz}(s, z = H_2, t) = -F^z_{2\to 1}. \quad \text{(B18)}$$

The average force per unit area is

$$f^z_{2\to 1} = \left\langle \frac{1}{A}F^z_{2\to 1}\right\rangle = -\left\langle \frac{1}{A}\frac{\partial}{\partial z}\sum_{i\in L_1}\sum_{j\in L_2}\Phi(s_{ij}, z)|_{z=H_2-H_1}\right\rangle$$
$$= P_{zz} \neq P_N. \quad \text{(B19)}$$

Equation (B19) for P_N is in full agreement with the derivation of the normal pressure for similar systems in Refs. [26,28–30].

If the z coordinates of the layers are fixed, as is the case in most of the computations in the present work, an external field compensates exactly the microscopic forces. In this case we have $H_1=-H_2=h/2$, $\dot{H}_1=\dot{H}_2=0$, and $\ddot{H}_1=\ddot{H}_2=0$ and the external forces are given by

$$F^z_{\text{ext},1} = \sum_{i\in L_1}\frac{\partial}{\partial z}\Phi_{\text{ext}}\left(s_i, \frac{h}{2}\right) = -F^z_{2\to 1} \quad \text{(B20)}$$

and

$$F^z_{\text{ext},2} = -F^z_{1\to 2} = F^z_{2\to 1} = -F^z_{\text{ext},1}. \quad \text{(B21)}$$

APPENDIX C: RECIPROCAL SPACE CONTRIBUTIONS TO THE PRESSURE TENSOR AND FORCES

The general formulas for the components of the stress tensor in terms of the interaction potential are given in Sec. II. In this appendix, we give explicit expressions for the reciprocal space contribution in an Ewald sum of the stress tensor components. They can be obtained directly from the results of Appendix A or from the general derivation given by Heyes [19] for quasi-two-dimensional systems.

The short-ranged contributions are easily obtained from Eqs. (A2) and (A3).

From Eq. (4) and with the notations of Appendix A, we have, for the bilayer system,

$$\Pi_T^{(dd,G)} = -\frac{1}{2A}\left\langle \sum_i s_i\cdot\nabla_{s_i}(E^{(\text{intra})}_{G\neq 0} + E^{(\text{inter})}_{G\neq 0})\right\rangle, \quad \text{(C1)}$$

$$P_{zz}^{(dd,G)} = -\frac{1}{A}\left\langle \frac{\partial}{\partial z}E^{(\text{inter})}_{G\neq 0}\Big|_{z=h}\right\rangle. \quad \text{(C2)}$$

The intralayer contributions to the lateral components of the stress tensor are given by

$$\sum_i s_i\cdot\nabla_{s_i}E^{(1,\text{intra})}_{G\neq 0} = -\frac{2\pi}{A}\sum_{G\neq 0}D(\alpha,G)\text{Im}\left[\left(\sum_{i\in L_1}(G\cdot s_i)\mu_i^z\exp(iG\cdot s_i)\right)\left(\sum_{i\in L_1}\mu_i^z\exp(iG\cdot s_i)\right)\right.$$
$$\left.+\left(\sum_{i\in L_2}(G\cdot s_i)\mu_i^z\exp(iG\cdot s_i)\right)\left(\sum_{i\in L_2}\mu_i^z\exp(iG\cdot s_i)\right)\right], \quad \text{(C3)}$$

$$\sum_i s_i\cdot\nabla_{s_i}E^{(2,\text{intra})}_{G\neq 0} = 0, \quad \text{(C4)}$$

$$\sum_i s_i\cdot\nabla_{s_i}E^{(3,\text{intra})}_{G\neq 0} = -\frac{2\pi}{A}\sum_{G\neq 0}H(\alpha,G)\text{Im}\left[\left(\sum_{i\in L_1}(G\cdot s_i)(\mu_i\cdot G)\exp(iG\cdot s_i)\right)\left(\sum_{i\in L_1}(\mu_i\cdot G)\exp(iG\cdot s_i)\right)\right.$$
$$\left.+\left(\sum_{i\in L_2}(G\cdot s_i)(\mu_i\cdot G)\exp(iG\cdot s_i)\right)\left(\sum_{i\in L_2}(\mu_i\cdot G)\exp(iG\cdot s_i)\right)\right], \quad \text{(C5)}$$

with functions D and H as defined in Eq. (A8).

Interlayer contributions are given by

$$\sum_i s_i\cdot\nabla_{s_i}E^{(1,\text{inter})}_{G\neq 0} = \frac{\pi}{A}\sum_{G\neq 0}I(\alpha,G;h)\text{Im}\left[\left(\sum_{i\in L_1}\mu_i^z\exp(iG\cdot s_i)\right)\left(\sum_{j\in L_2}\mu_j^z(G\cdot s_j)\exp(-iG\cdot s_j)\right)\right.$$
$$\left.-\left(\sum_{i\in L_1}\mu_i^z(G\cdot s_i)\exp(iG\cdot s_i)\right)\left(\sum_{j\in L_2}\mu_j^z\exp(-iG\cdot s_j)\right)\right], \quad \text{(C6)}$$

$$\sum_i s_i\cdot\nabla_{s_i}E^{(2,\text{inter})}_{G\neq 0} = \frac{\pi}{A}\sum_{G\neq 0}J(\alpha,G;h)\text{Re}\left[\left(\sum_{i\in L_1}\mu_i^z(G\cdot s_i)\exp(iG\cdot s_i)\right)\left(\sum_{j\in L_2}(\mu_j\cdot G)\exp(-iG\cdot s_j)\right)-\left(\sum_{i\in L_1}\mu_i^z\exp(iG\cdot s_i)\right)\right.$$
$$\times\left(\sum_{j\in L_2}(\mu_j\cdot G)(G\cdot s_j)\exp(-iG\cdot s_j)\right)+\left(\sum_{i\in L_1}(\mu_i\cdot G)(G\cdot s_i)\exp(iG\cdot s_i)\right)\left(\sum_{j\in L_2}\mu_j^z\exp(-iG\cdot s_j)\right)$$
$$\left.-\left(\sum_{i\in L_1}(\mu_i\cdot G)\exp(iG\cdot s_i)\right)\left(\sum_{j\in L_2}\mu_j^z(G\cdot s_j)\exp(-iG\cdot s_j)\right)\right], \quad \text{(C7)}$$

$$\sum_i \boldsymbol{s}_i \cdot \boldsymbol{\nabla}_{\boldsymbol{s}_i} E^{(3,\mathrm{inter})}_{\boldsymbol{G}\neq 0} = -\frac{\pi}{A}\sum_{\boldsymbol{G}\neq \boldsymbol{0}} K(\alpha,G;h)\mathrm{Im}\left[\left(\sum_{i\in L_1}(\boldsymbol{\mu}_i\cdot\boldsymbol{G})(\boldsymbol{G}\cdot\boldsymbol{s}_i)\exp(i\boldsymbol{G}\cdot\boldsymbol{s}_i)\right)\left(\sum_{j\in L_2}(\boldsymbol{\mu}_j\cdot\boldsymbol{G})\exp(-i\boldsymbol{G}\cdot\boldsymbol{s}_j)\right)\right.$$
$$\left. -\left(\sum_{i\in L_1}(\boldsymbol{\mu}_i\cdot\boldsymbol{G})\exp(i\boldsymbol{G}\cdot\boldsymbol{s}_i)\right)\left(\sum_{j\in L_2}(\boldsymbol{\mu}_j\cdot\boldsymbol{G})(\boldsymbol{G}\cdot\boldsymbol{s}_j)\exp(-i\boldsymbol{G}\cdot\boldsymbol{s}_j)\right)\right], \tag{C8}$$

with functions I, J, and K defined in Eq. (A5).

The contributions to the normal component of the stress tensor are given by

$$\left.\frac{\partial}{\partial z}E^{(1,\mathrm{inter})}_{\boldsymbol{G}\neq 0}\right|_{z=h} = -\frac{\pi}{A}\sum_{\boldsymbol{G}\neq 0}\left(G^2 J(\alpha,G;h)+\frac{4\alpha^3 h}{\sqrt{\pi}}Q(\alpha,G;h)\right)\mathrm{Re}\left[\left(\sum_{i\in L_1}\mu_i^z\exp(i\boldsymbol{G}\cdot\boldsymbol{s}_i)\right)\left(\sum_{j\in L_2}\mu_j^z\exp(-i\boldsymbol{G}\cdot\boldsymbol{s}_j)\right)\right], \tag{C9}$$

$$\left.\frac{\partial}{\partial z}E^{(2,\mathrm{inter})}_{\boldsymbol{G}\neq 0}\right|_{z=h} = \frac{\pi}{A}\sum_{\boldsymbol{G}\neq 0}\left(G^2 K(\alpha,G;h)-\frac{2\alpha}{\sqrt{\pi}}P(\alpha,G;h)\right)\mathrm{Im}\left[\left(\sum_{i\in L_1}(\boldsymbol{\mu}_i\cdot\boldsymbol{G})\exp(i\boldsymbol{G}\cdot\boldsymbol{s}_i)\right)\left(\sum_{j\in L_2}\mu_j^z\exp(-i\boldsymbol{G}\cdot\boldsymbol{s}_j)\right)\right.$$
$$\left.+\left(\sum_{i\in L_1}\mu_i^z\exp(i\boldsymbol{G}\cdot\boldsymbol{s}_i)\right)\left(\sum_{j\in L_2}(\boldsymbol{\mu}_j\cdot\boldsymbol{G})\exp(-i\boldsymbol{G}\cdot\boldsymbol{s}_j)\right)\right], \tag{C10}$$

$$\left.\frac{\partial}{\partial z}E^{(3,\mathrm{inter})}_{\boldsymbol{G}\neq 0}\right|_{z=h} = \frac{\pi}{A}\sum_{\boldsymbol{G}\neq 0}\mathrm{J}(\alpha,G;h)\mathrm{Re}\left[\left(\sum_{i\in L_1}(\boldsymbol{\mu}_i\cdot\boldsymbol{G})\exp(i\boldsymbol{G}\cdot\boldsymbol{s}_i)\right)\left(\sum_{j\in L_2}(\boldsymbol{\mu}_j\cdot\boldsymbol{G})\exp(-i\boldsymbol{G}\cdot\boldsymbol{s}_j)\right)\right]. \tag{C11}$$

The function $Q(\alpha,G;h)$ is obtained from the derivative of J, i.e.,

$$Q(\alpha,G;h) = 2\exp\left(-\frac{G^2}{4\alpha^2}\right)\exp(-\alpha^2 h^2). \tag{C12}$$

Finally,

$$\left.\frac{\partial}{\partial z}E^{(\mathrm{inter})}_{\boldsymbol{G}=0}\right|_{z=h} = -2\alpha^2 h E^{(\mathrm{inter})}_{\boldsymbol{G}=0} \tag{C13}$$

with $E^{(\mathrm{inter})}_{\boldsymbol{G}=0}$ given by Eq. (A6).

[1] J.-J. Weis, J. Phys.: Condens. Matter **15**, S1471 (2003), and references therein.
[2] L. Saiz and M. L. Klein, Acc. Chem. Res. **35**, 482 (2002).
[3] H. L. Scott, Curr. Opin. Struct. Biol. **12**, 495 (2002).
[4] K. De'Bell, A. B. MacIsaac, and J. P. Whitehead, Rev. Mod. Phys. **72**, 225 (2000).
[5] A. Pertsin, D. Platonov, and M. Grunze, Langmuir **23**, 1388 (2007), and references therein.
[6] M. Klokkenburg, C. Vonk, E. M. Claessen, J. D. Meeldijk, B. H. Erné, and A. P. Philipse, J. Am. Chem. Soc. **126**, 16706 (2004).
[7] M. Klokkenburg, R. P. A. Dullens, W. K. Kegel, B. H. Erné, and A. P. Philipse, Phys. Rev. Lett. **96**, 037203 (2006).
[8] M. Klokkenburg, B. H. Erné, J. D. Meeldijk, A. Wiedenmann, A. V. Petukhov, R. P. A. Dullens, and A. P. Philipse, Phys. Rev. Lett. **97**, 185702 (2006).
[9] J.-J. Weis, J. M. Tavares, and M. M. Telo da Gama, J. Phys.: Condens. Matter **14**, 9171 (2002).
[10] J. M. Tavares, J.-J. Weis, and M. M. Telo da Gama, Phys. Rev. E **65**, 061201 (2002).
[11] J. M. Tavares, J.-J. Weis, and M. M. Telo da Gama, Phys. Rev. E **73**, 041507 (2006).
[12] J.-J. Weis, Mol. Phys. **100**, 579 (2002).
[13] A. Satoh, R. W. Chantrell, S. I. Kamiyama, and G. N. Coverdale, J. Colloid Interface Sci. **178**, 620 (1996).
[14] E. Lomba, F. Lado, and J.-J. Weis, Phys. Rev. E **61**, 3838 (2000).
[15] J.-J. Weis, Mol. Phys. **103**, 7 (2005).
[16] P. D. Duncan and P. J. Camp, J. Chem. Phys. **121**, 11322 (2004).
[17] A. Yu. Zubarev and L. Yu. Iskakova, Phys. Rev. E **76**, 061405 (2007).
[18] T. Kristóf and I. Szalai, Phys. Rev. E **72**, 041105 (2005).
[19] D. M. Heyes, Phys. Rev. B **49**, 755 (1994).
[20] A. Grzybowski, E. Gwóźdź, and A. Bródka, Phys. Rev. B **61**, 6706 (2000).
[21] J.-J. Weis and D. Levesque, in *Advanced Computer Simulation Approaches for Soft Matter Sciences II*, edited by C. Holm and K. Kremer, Advances in Polymer Science Vol. 185 (Springer, New York, 2005).
[22] J.-J. Weis, D. Levesque, and S. Jorge, Phys. Rev. B **63**, 045308 (2001).
[23] M. Mazars, Mol. Phys. **103**, 1241 (2005).
[24] M. Mazars, Mol. Phys. **105**, 1909 (2007).
[25] V. I. Valtchinov, G. Kalman, and K. B. Blagoev, Phys. Rev. E **56**, 4351 (1997).

[26] J. S. Rowlinson and B. Widom, *Molecular Theory of Capillarity* (Clarendon Press, Oxford, 1982).
[27] A. Santos, M. López de Haro, and S. Bravo Yuste, J. Chem. Phys. **103**, 4622 (1995).
[28] (a) P. Schofield and J. R. Henderson, Proc. R. Soc. London, Ser. A **379**, 231 (1982); (b) J. H. Irving and J. G. Kirkwood, J. Chem. Phys. **18**, 817 (1950); (c) J. G. Kirkwood and F. P. Buff, *ibid.* **17**, 338 (1949).
[29] J. P. R. B. Walton and K. E. Gubbins, Mol. Phys. **55**, 679 (1985).
[30] S. H. L. Klapp and M. Schoen, J. Chem. Phys. **117**, 8050 (2002).
[31] R. Shuttleworth, Proc. Phys. Soc., London, Sect. A **63**, 444 (1950).
[32] L. Blum and A. J. Torruella, J. Chem. Phys. **56**, 303 (1972).
[33] C. G. Gray and K. E. Gubbins, *Theory of Molecular Liquids* (Clarendon Press, Oxford, 1984).
[34] G. N. Patey, Mol. Phys. **34**, 427 (1977).
[35] P. Attard and D. J. Mitchell, Chem. Phys. Lett. **133**, 347 (1987).
[36] P. Attard and D. J. Mitchell, J. Chem. Phys. **88**, 4391 (1988).
[37] R. Eppenga and D. Frenkel, Mol. Phys. **52**, 1303 (1984).
[38] A. Carbognani, E. Rastelli, S. Regina, and A. Tassi, Phys. Rev. B **62**, 1015 (2000).
[39] Yu. M. Malozovsky and V. M. Rozenbaum, Physica A **175**, 127 (1991).
[40] E. Rastelli, S. Regina, A. Tassi, and A. Carbognani, Phys. Rev. B **65**, 094412 (2002).
[41] P. Politi, M.G. Pini, and R.L. Stamps, Phys. Rev. B **73**, 020405(R) (2006).
[42] B. Jönsson and H. Wennerström, J. Chem. Soc., Faraday Trans. 2 **79**, 19 (1983).
[43] M. Granfeldt, B. Jönsson, and H. Wennerström, Mol. Phys. **64**, 129 (1988).
[44] R. P. Rand and V. A. Parsegian, Biochim. Biophys. Acta **988**, 351 (1989).
[45] B. Jönsson, P. Attard, and D. J. Mitchell, J. Phys. Chem. **92**, 5001 (1988).